REVIEW

Check for updates

A review of the microwave-assisted synthesis of carbon nanomaterials, metal oxides/hydroxides and their composites for energy storage applications

Nitika Devi,[a,b] Sumanta Sahoo, [ID][c] Rajesh Kumar [ID] *[d] and Rajesh Kumar Singh [ID] *[a]

Currently, nanomaterials are considered to be the backbone of modern civilization. Especially in the energy sector, nanomaterials (mainly, carbon- and metal oxide/hydroxide-based nanomaterials) have contributed significantly. Among the various green approaches for the synthesis of these nanomaterials, the microwave-assisted approach has attracted significant research interest worldwide. In this context, it is noteworthy to mention that because of their enhanced surface area, high conducting nature, and excellent electrical and electrochemical properties, carbon nanomaterials are being extensively utilized as efficient electrode materials for both supercapacitors and secondary batteries. In this review article, we briefly demonstrate the characteristics of microwave-synthesized nanomaterials for next-generation energy storage devices. Starting with the basics of microwave heating, herein, we illustrate the past and present status of microwave chemistry for energy-related applications, and finally present a brief outlook and concluding remarks. We hope that this review article will positively convey new insights for the microwave synthesis of nanomaterials for energy storage applications.

1. Introduction

Clean and renewable energy-related achievements and issues are highly concerning aspects in the 21st century due to the increasing pollution, and consequently enhancement in global warming on the Earth.[1–5] The emission of harmful gases from factories and combustion from vehicles due to use of limited fossil fuel are one of the main reasons for the presence of greenhouse gases in the atmosphere, air pollution and climate change.[6–9] Also, due to the increasing population worldwide, the consumption of limited fossil fuels is increasing continuously, and pollution is an unavoidable issue in the foreseeable future, which are the biggest challenges in society. Considering these unavoidable harmful issues and the threat to human life associated with environmental pollution, attention is focused on the design of value-added and cost-effective

materials as electrodes for efficient utilization in energy storage and conversion processes.[10–21]

Among the energy storage devices, supercapacitors and secondary batteries have attracted widespread attention from researchers and are considered potential energy devices due to their good energy/power storage capacity, ultra-long term cycling stability, flexible operating temperature and environmentally friendly nature.[22–25] In energy storage devices, the energy density, power density and robust cyclability properties are significant indicators to evaluate their performance.[26–35] To improve these properties in energy storage devices, the performance of supercapacitors and batteries depend highly on the nature of electrode materials. For electrode materials, researchers have developed various high surface area carbon materials and metal oxide/hydroxide-based composites/hybrids. Recently, carbon materials modified with metal oxides/hydroxides using various methods have been utilized as energy storage electrodes in supercapacitors and secondary batteries.[36–52]

Nowadays, with continuous development in nanomaterial synthesis, the microwave (MW)-assisted approach has attracted significant attention from researchers due to its uniform heating inside materials.[53–58] This is also because of the exceptional features of MW heating such as fast synthesis, selective heating without interaction with the surroundings and cost efficiency. MW generates direct volumetric heating and heat is simultaneously produced in the whole system, which results in

[a]School of Physical and Material Sciences, Central University of Himachal Pradesh (CUHP), Dharamshala, Kangra, HP-176215, India. E-mail: rksbhu@gmail.com
[b]School of Physics & Materials Science, Shoolini University, Solan, Himachal Pradesh 173229, India
[c]Department of Chemistry, Madanapalle Institute of Technology and Science, Madanapalle, Andhra Pradesh, 517325, India
[d]Advanced Nanoengineering Materials Laboratory, Department of Mechanical Engineering, Indian Institute of Technology Kanpur, Kanpur-208016, India. E-mail: rajeshbhu1@gmail.com

fast heating.[59–65] Selective heating can be performed during synthesis and is controlled due to the dielectric properties of materials.[66–75] Nowadays, MW-irradiation (MWI) is frequently utilized for the synthesis of various types of carbon materials, metal oxides and metal hydroxides for energy-related electrode materials. Initially, the use of MWI was limited to inorganic synthesis and not used for organic synthesis. This is because of the non-polar nature of organic solvents, which do not support dielectric heating. However, nowadays several alternatives for this problem have been invented.[76] In the case of carbon materials, the interaction mechanism is different from dielectric heating. In carbon materials, free electrons play a crucial role in heating.[77] Fig. 1 shows a schematic representation for the use of MW for the synthesis of carbon-based and metal oxide/hydroxide-containing materials for energy storage electrodes.

In energy conversion devices, the MW-assisted approach has also been applied for the synthesis of carbon-modified electrodes materials for fuel cells.[78–85] MW-assisted synthesis was employed to obtain a carbon black-supported polytetrafluoroethylene (PTFE/C) nanocomposite, which delivered an output power of 0.66 W cm^{-2}.[81] The Pt/carbon nanotube (CNT) composite obtained *via* MW-assisted synthesis was used as a high-performing catalyst for the oxygen reduction reaction in a proton-exchange membrane fuel cell.[82] Carbon-supported ternary Pt–Sn–Rh alloy nanoparticles were synthesized using MW and applied for fuel cells, displaying good mass activities (2.18 A mg$_{Pt}^{-1}$ and 1.70 A mg$_{Pt}^{-1}$) for the ethanol and methanol oxidation reaction, which were 5.7 and 3.7 times greater than that of a commercial Pt/C catalyst, respectively.[83] Recently, N-doped and oxygen-functionalized carbon nanoonion-supported Pd nanoparticles were synthesized *via* MW and used as an electrocatalyst, which exhibited a good current density (17.4 mA cm^{-2}), long-term stability (6.9 mA cm^{-2}), and fast electron transfer towards the ethanol oxidation reaction in alkaline medium.[84] A reduced graphene oxide (rGO)-CuS-ZnS hybrid nanocomposite was synthesized *via* MW and used as a cathode, exhibiting a power generation of 1692 ± 15 mW m^{-2} and open circuit potential of 761 ± 9 mV.[85]

MWI is electromagnetic waves and prominently used in the telecommunication industry and its wavelength spectrum range appears between radio waves and the infrared region. The MW wavelengths in this range are from 1 m to 1 mm and the corresponding frequency is 0.3 GHz to 300 GHz. Domestic MW ovens (kitchen MW ovens) function at the frequency of 2.45 GHz, which is already in the range 0.3–300 GHz. Also, MWI plays an important role in scientific research especially in materials science for the synthesis of materials.[86–94]

2. Microwave: simple and fast approach

MWI provides much faster heat distribution compared to conventional heating due to its unique volumetric heating in

Nitika Devi is an Asst. Professor in the Department of Physics & Materials Science, Shoolini University, Himachal Pradesh, India. She has done M.Sc. physics (2015) from Himachal Pradesh University, Shimla. She obtained her Ph.D. degree in Physics (2021) from Central University of Himachal Pradesh. She has been working in the area of energy storage devices such as fuel cells, supercapacitors, batteries and also on the synthesis and application of carbon materials and its composites based on carbon nanotubes, graphene and their derivatives.

Nitika Devi

Dr Sumanta Sahoo is working as an Asst. Professor in Madanapalle Institute of Technology & Science, Andhra Pradesh, India. He got his Ph.D. degree in Materials Science from the Materials Science Centre, Indian Institute of Technology Kharagpur (I.I.T. Kharagpur), West Bengal, India. He worked at the Korea Advanced Institute of Science and Technology (KAIST) (Graphene Research Center: Postdoctoral researcher: 2013–2014) Daejeon, South Korea, Yeungnam University (School of Chemical Engineering; International Research Professor: 2015–2017), Daegu, South Korea, and Indian Institute of Technology, Dhanbad, Jharkhand, India (Department of Chemistry; National Postdoctoral Fellow: 2018–2019). Dr Sahoo is an active researcher in the field of graphene, MXene, supercapacitor electrodes based on graphene, conducting polymers, and metal oxides/mixed metal oxides; and ternary nanocomposites for Li-ion batteries and fabrication of asymmetric supercapacitor devices. Dr Sahoo has published 53 peer-reviewed research/review articles in refereed international journals and 2 book chapters. According to the Google Scholar site, Dr. Sahoo has total citations of 2131 with the h-index of 26 and i-10 index of 40.

Sumanta Sahoo

materials. Heating by MWI is different from conventional heating in which heating occurs by conduction and convection processes. Also, MWI-assisted heating is a cost-efficient approach for laboratory synthesis and domestic use.[95–98] Fig. 2 presents a schematic comparison of the temperature distribution profile and heat transfer during MW-assisted and conventional heating. In MW-assisted heating, initially the particle interior is hotter than the particle surface. In MW-assisted heating, a temperature gradient occurs from the centre to the particle surface, whereas in conventional heating, a temperature gradient occurs from the particle surface to the centre. Thus, in MW-assisted heating, (*e.g.*, under pyrolysis conditions), the volatile matter moves from the higher-temperature particle interior to the lower-temperature surface.[99–102]

2.1.   Microwave heating: mechanism

MW heating mechanism is mainly dependent on the nature of the irradiated/exposed materials. The MW interaction is extremely dependent on the nature of the material and the degree of interaction. It is different for conductors, insulators, and dielectric materials.[103] Three types of mechanisms have been mentioned in the literature when a material is irradiated/exposed to MWI. The common interaction phenomena are reflection, absorption and transmittance. Electrical conductors such as metals are reflectors of MWI. Some materials (quartz and PTFE) allow the transmission of MWI. Thus, conductors cannot be heated by MWs because they do not absorb MWI. However, polar liquids containing molecules and polar molecules are good absorbers of MW radiation, and consequently heat very quickly after MWI due to dipolar interactions and ionic conduction.[103,104] When different dipoles and ions interact with electromagnetic waves, they accelerate with the frequency of the electromagnetic waves. Both ions and dipoles try to flip their orientation with the frequency of the electromagnetic waves. In both cases, flipping of their orientation is delayed due to the frictional forces of the surrounding ions

Rajesh Kumar

Dr Rajesh Kumar is Ramanujan Fellow in the Indian Institute of Technology, Kanpur (I.I.T. Kanpur), India. Previously, he was an International JSPS (Japan Society for the Promotion of Sciences) (standard) Postdoctoral Fellow (2018–2020) in Toyohashi University of Technology, Toyohashi, Japan. He obtained his B.Sc. and M.Sc. (Physics) Degrees from Allahabad University, Allahabad, India. After that he received his Ph.D. degree in Physics from the Department of Physics, Banaras Hindu University (B.H.U.), Varanasi, India. Soon after completing his Ph. D., he joined the Korea Advanced Institute of Science and Technology (KAIST) (Graphene Research Center), Daejeon, South Korea (May 2012–May 2014) to carry out postdoctoral research. Afterward, he moved to the Department of Materials Science and Engineering, Yonsei University, Seoul, South Korea to work as a Brain Korea 21 (BK-21) Research Professor. In 2015, he joined the Centre for Semiconductor Components and Nanotechnology, University of Campinas (UNICAMP), Campinas, Brazil as a CNPq postdoctoral fellow/visiting scientist (Mar. 2015–Dec. 2017). In Sept 2017, he got distinguished FAPESP (Sao Paulo Research Foundation Fellowship) postdoctoral fellowship and moved (Jan 2018) to the State University of Sao Paulo, Presidente Prudente, Brazil. Dr Kumar is serving as an editorial board member and reviewer for several journals of international repute. Dr Kumar has published 8 international book chapters and more than 75 research/review articles in peer-reviewed SCI refereed international journals. His main research interests are synthesis of 2D layered materials (graphene based materials/inorganic layered materials) for energy related applications.

Rajesh Kumar Singh

Dr Rajesh Kumar Singh is an Asst. Professor in the School of Physical and Material Sciences, Central University of Himachal Pradesh, Himachal Pradesh, India. He obtained his Ph.D. Degree in Physics from the Institute of Sciences, Banaras Hindu University (B.H.U) Varanasi, India. He then spent 4 years (2011–2015) at the Indian Institute of Technology (B.H.U.) Varanasi as a Postdoctoral Fellow. His current research interests include hydrogen storage materials, solid oxide fuel cells, Supercapacitors, Li-ion batteries and synthesis of carbon nano-structures-metal/metal oxide self-assembly and their applications in various energy related areas. Dr Singh has published more than 70 peer reviewed international research/review articles including 4 book chapters.
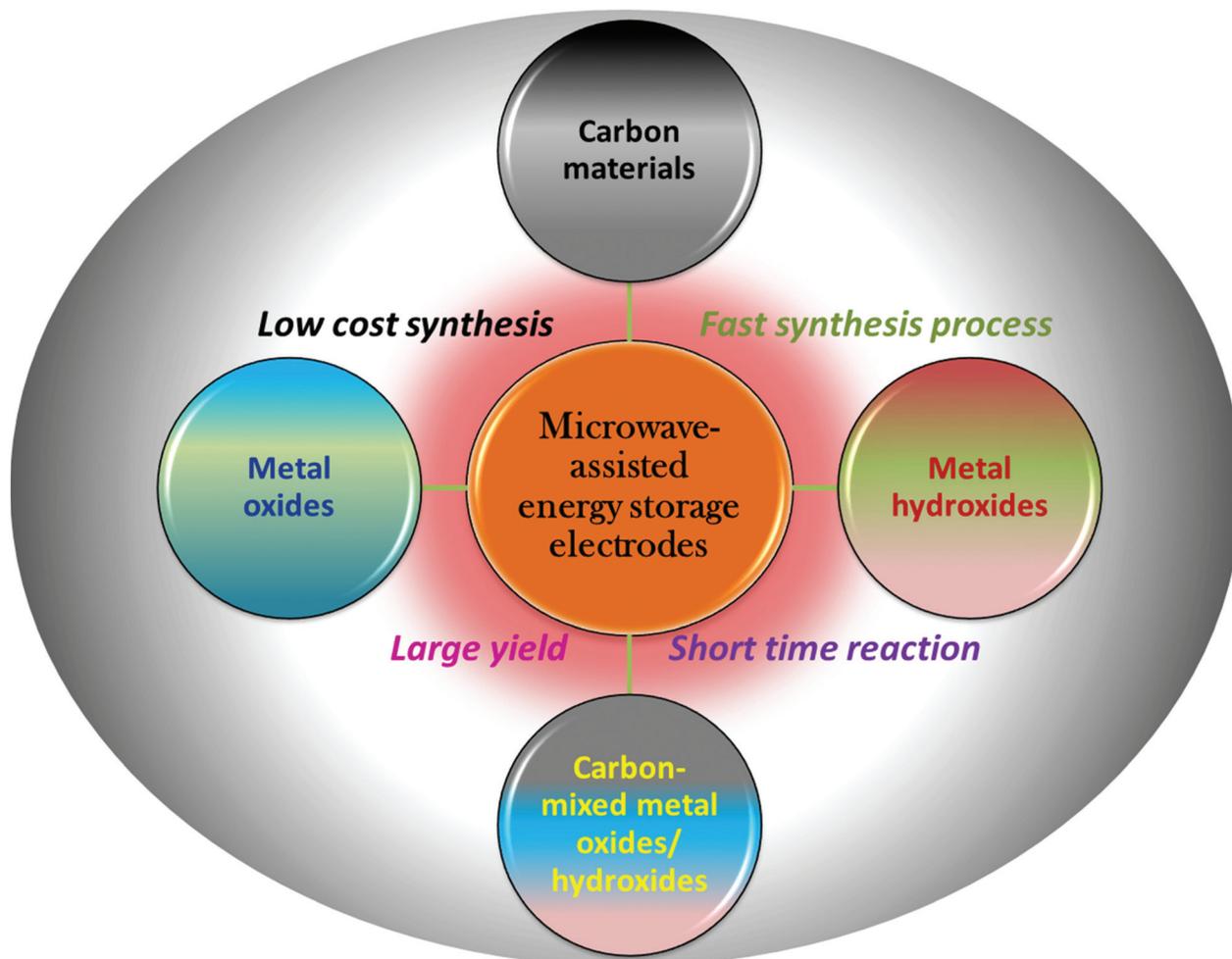
Fig. 1 Schematic illustration of the use of MW-assisted synthesis of energy storage materials and its advantage.
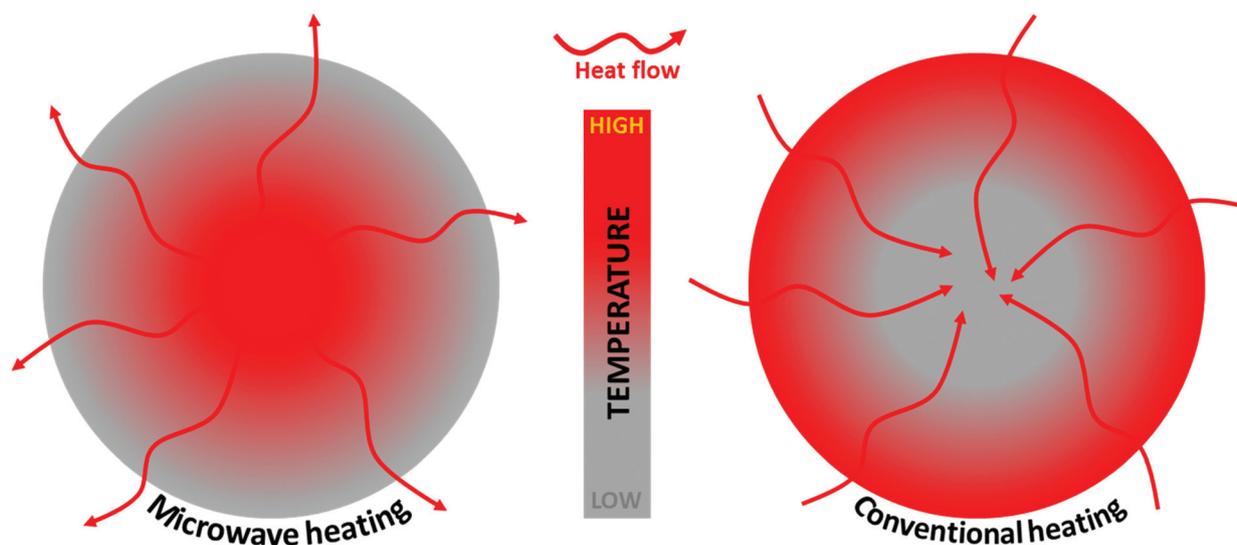

Fig. 2 Schematic representation of the temperature gradient and heat flow due to MW and conventional heating.

and dipoles. This delay is called the relaxation time, and the energy losses during this period are liberated as heat, which spreads inside and uniformly heats the material. MW heating depends on some factors among which the dielectric parameter is crucial. The penetration depth is another important factor for the heating of materials, which is defined as[103,104]

$$D = \frac{c\varepsilon^{\circ}}{2\pi f \varepsilon'} \tag{1}$$

where f is the frequency, c is the capacitance and ε° is the dielectric constant of free space. It can be seen from this equation that the penetration depth increases with an increase in capacitance and decrease in frequency. In case of an MW reflector (conducting medium is metal), the penetration depth becomes null because the capacitance for metal is zero. If the penetration depth is infinite, it means that MWs transmit from the materials without any absorption. Two other important quantities for defining the dielectric properties of materials are the loss tangent (δ) and dielectric constant. The dielectric constant (ε) of a material is the sum of the real (ε') and imaginary permittivity (ε''). It can be written as follows:

$$\varepsilon = \varepsilon' + \varepsilon'' \tag{2}$$

The real part of the dielectric constant deals with the absorbance of MW radiation and the imaginary part deals with loss.

The MW absorption ability of a material is generally defined by the loss tangent, which can be written as[95,96,103–105]

$$\tan \delta = \varepsilon'/\varepsilon'' \tag{3}$$

A large loss tangent value means good MW absorption, and thus the material characteristics such as penetration depth, dielectric constant and loss tangent should be carefully studied before the selection of materials for MW absorbance.

Fig. 3 shows the transmission, absorption and reflection of some materials, which are defined by the dielectric loss factor and power absorbed. According to Fig. 3, it can be concluded that the materials present between two extreme values of dielectric loss factor are best for MW absorption. In many chemistry reactions assisted by MWI and heating, they mainly depend on the solvents involved. Thus, there are some common solvents that are being used. The common solvents with their loss tangent values and dielectric constants are presented in Table 1. It can be seen that there is a corresponding increase in loss tangent with an increase in the dielectric constant. Thus, the selection of a particular solvent is required to maintain the heat for a desired reaction. Depending on the values of $\tan \delta$, the solvents are classified as (i) $\tan \delta > 0.5$, higher MW absorption solvent, (ii) $\tan \delta > 0.1$, medium MW absorption solvent, and (iii) $\tan \delta < 0.1$, low MW absorption solvent.[76]
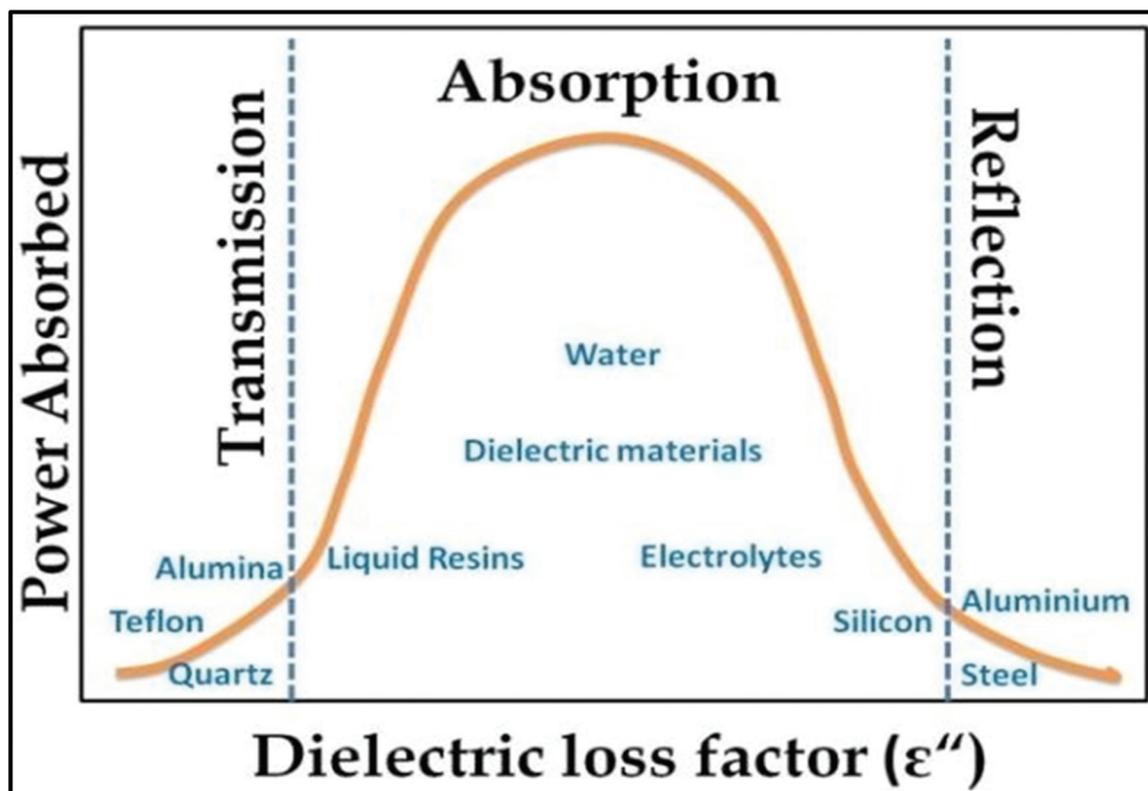

Fig. 3 Dependence of reflection, absorption and transmittance on dielectric loss factor process.[97] Reprinted (adapted) with permission from ref. 97, copyright (1999), Elsevier B.V. All rights reserved.

Table 1 Some important solvents with their dielectric constant and loss tangent values[106]

Solvent	Dielectric constant	Loss tangent (tan δ)
Hexane	1.9	—
Benzene	2.3	—
Carbon tetrachloride	2.2	—
Chloroform	4.8	0.091
Acetic acid	6.1	0.174
Ethyl acetate	6.2	0.059
THF	7.6	0.047
Methylene chloride	9.1	0.042
Acetone	20.6	0.054
Ethanol	24.6	0.941
Methanol	32.7	0.659
Acetonitrile	36.0	0.062
Dimethylformamide	36.7	0.161
Dimethylsulfoxide	47.0	0.825
Formic acid	58.0	0.722
Water	80.4	0.123

2.2. Microwave *versus* conventional thermal heating

MW heating provides several advantages compared to conventional heating due to its fast, uniform heating, cost efficiency and reduced energy consumption. MW heating is a volumetric heating, which means the material absorbs radiation and directly converts it into heat. Conversely, in the case of conventional thermal heating, heating takes place *via* conduction and convection processes and is transferred from the surface to molecules. Also, MW radiation relies on dielectric heating, which gives rise to selective heating. Past studies have shown a comparison between MW and conventional heating in the synthesis of materials. Ma *et al.*[107] studied the synthesis of BaTiO$_3$ *via* MW and conventional heating and suggested that MW heating gives rise to a larger *c/a* ratio (lattice parameters) and needs shorter time for crystallization. MWI has been used in different synthetic processes, especially to achieve uniform and selective heating. MW radiation is preferably used in the powder metallurgy and ceramic fields for sintering processes. Sintering by MW heating offers good physical and mechanical strength, reduced energy consumption and shorter reaction duration. Oghbaei *et al.*[108] explained the difference between MW and conventional sintering and discussed the basic aspects of MW heating and conventional heating.[109] Volumetric heating results in uniform heating, whereas conventional heating has a temperature gradient, which is not good for mechanical strength and homogeneous morphology in materials. Also, inorganic and organic reactions can occur at much faster rates with MW heating compared to conventional heating.[96,110] Berlan *et al.*[111] studied the reaction rates for the cycloaddition reaction performed in xylene or dibutylether and found that the effects were more pronounced in the case of polar solvents. A schematic representation of the reaction is shown in Fig. 4a.
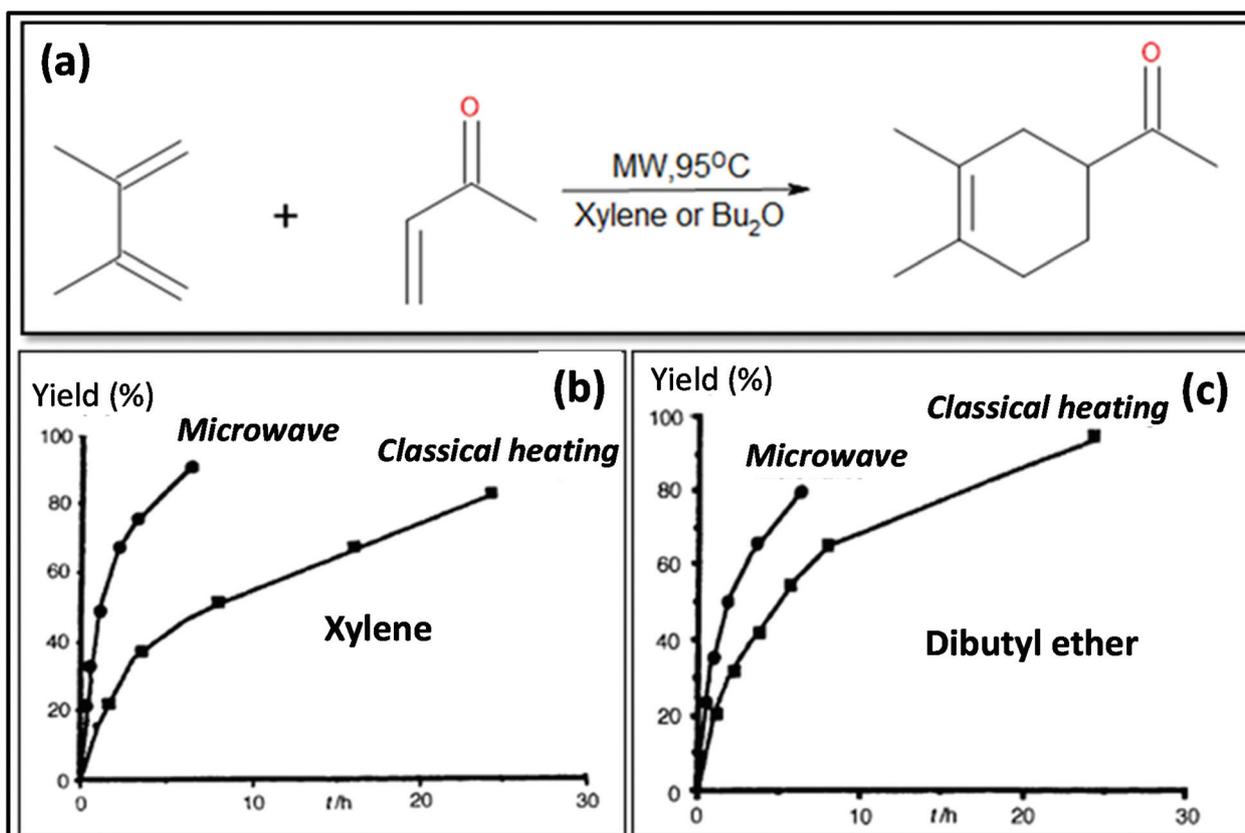
Fig. 4 (a) Schematic molecular representation and MW condition. (b) and (c) Effects of different types of heating on product yield for xylene and dibutyl ether.[111] Reprinted (adapted) with permission from ref. 111, copyright (1991), Elsevier B.V. All rights reserved.

The effect of different heating processing on the yield of the reaction mixture is shown in Fig. 4b and c. It can be seen from Fig. 4b and c that for xylene and dibutyl ether, MW heating resulted in a large product yield in a shorter time compared to conventional heating.[111]

Hydrolysis of adenosine triphosphate showed a 25-times faster rate using MW heating compared to conventional heating.[112] MW heating increases the kinetic energy of the solvent through volumetric heating and hydrolysis completely depends on the temperature of the reaction mixture (not on the heating method), where the temperature was better controlled by MW heating.[112] In addition to increase the reaction rate, one can also achieve selective product by controlling the power of the MW radiation. The Arrhenius kinetic model can be written as[113]

$$R_1 + R_2 \overset{K1,E1}{\Leftrightarrow} P_1 \qquad (4)$$

$$R_1 + R_3 \overset{K2,E2}{\Leftrightarrow} P_2 \qquad (5)$$

Applying conventional heating, the obtained product is a mixture of P_1 and P_2, but after increasing the heating rate by using MW heating, it is possible to produce product P_1 only by adding reagents R_1, R_2 and R_3. This type of situation is called induced heating, as shown in Fig. 5a. There is another possibility, which is called inversion heating, where careful control and fast heating gives rise to product P_2, but in the case of conventional heating, essentially product P_1 can be obtained. The inversion heating condition is shown in Fig. 5b.[113] Thus, reactivity can be changed by selective heating.

Thus, it can be concluded that MW heating gives rise to uniform heating and better selective product yield. These characteristics of MW radiation make it useful for synthesis *via* inorganic and organic chemical reactions.

3. Microwave-assisted synthesis

MW radiation is conventionally used for the synthesis of various materials such as carbon materials, metal oxides, and metal hydroxides and other organic/inorganic materials. The interactions of MW radiation is different for various types of materials.

3.1. Carbon nanomaterials

Carbon nanomaterials are good absorbers of MW and interact in different ways with MWI, which is different from the dielectric heating phenomenon. In the case of carbon nanomaterials, the large numbers of free electrons available in these materials are responsible for heating after MWI. When electromagnetic radiation interacts with electrons, the electrons try to oscillate with the same phase of electromagnetic radiation, but the radiation changes their phase very quickly and oscillating electrons cannot match with the same phase. This phase lag results in energy dissipation in the form of heat inside carbon materials. Other interesting phenomena also occur during MWI, when the kinetic energy of an electron increases, it causes a spark, and consequently ionization in the surrounding in the form of plasma.[77,114] Accordingly, carbon nanomaterials can be easily modified with metal oxides *via* MWI to form composite/hybrid structures. Devi *et al.*[115] reported the MW-assisted synthesis of graphene and its derivative and concluded that MWI can be effectively applied for these syntheses. The dielectric loss factors of some carbon materials are presented in Table 2. Due to their good absorption of MW, carbon materials can also be used in other applications as a heat receptor.[77]

The good absorbing nature of carbon materials has been utilized in processes such as the pyrolysis of biomass and waste[77,129,130] and soil remediation.[131,132] Here carbon materials are used as a receptor for MW radiation to provide
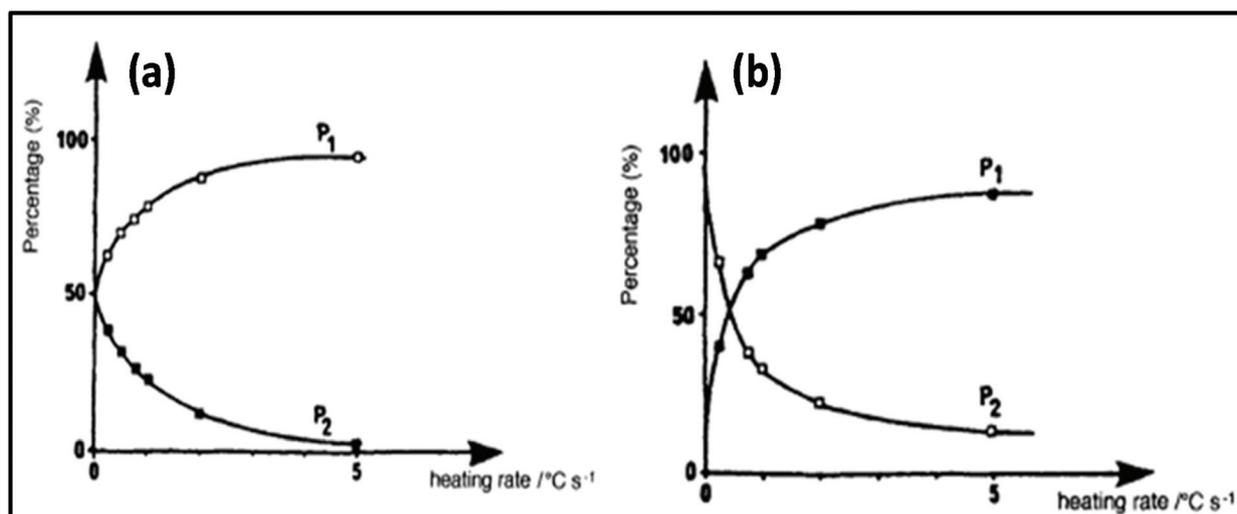

Fig. 5 Controlling rate of reaction using MW heating: (a) induced heating and (b) inversion heating.[113] Reprinted (adapted) with permission from ref. 113, copyright (1993), Elsevier B.V. All rights reserved.

Table 2 Dielectric loss factor of some carbon materials at a frequency of 2.45 GHz and at room temperature, 298 K (ref. 77)

Carbon material	tan δ	Ref.
Coal	0.02–0.08	116 and 117
Carbon foam	0.05–0.20	118
Charcoal	0.11–0.29	119 and 120
Carbon black	0.35–0.83	121 and 122
Activated carbon	0.57–0.80	119, 123 and 124
Activated carbon	0.22–2.95	125
Carbon nanotube	0.25–1.14	126 and 127
CSi nanofibres	0.58–1.00	128

the required heating temperature for these reactions. Accordingly, carbon materials make these synthetic processes less time consuming, reducing the energy consumption.[133–135] The production of carbon nanofilaments is an example of these processes, which previously involved expensive and long processes. For the synthesis of carbon nanofilaments, activated carbon was irradiated by MW in the presence of CH_4/N_2 and CH_4/CO_2. In both cases, activated carbon acts as both a catalyst and receptor.[136,137] The production of nanofilaments is not possible *via* the conventional heating method. This is because MW heating encourages the formation of nanofilaments in an entirely different way that is not possible with conventional heating. Ko *et al.*[138] employed MW radiation for the purification of carbon nanotubes in nitric acid. The functionalization of carbon nanotubes takes a long time and involves many steps. This problem can also be solved by using MW-assisted functionalization. Reactions such as amidation and 1,3-dipolar cycloaddition for the functionalization of carbon nanotubes can be done within 15 min. The additional advantages of using MW heating for functionalization is no need for the use of toxic agents, uniform dispersion and undamaged carbon nanotubes.[139] MW heating has also been used for the production of many carbon-based products from graphite such as isotropic anisotropic pitch-based carbon powder, expanded graphite with a layered structure having a larger interlayer separation than the natural graphite,[140] and synthesis of ordered mesoporous graphite carbon materials. MW heating also makes the conventionally used hydrothermal and sol–gel processes much simpler and faster.[141] Traditionally, activated carbon is produced *via* the activation of organic precursors at high temperatures up to 1173 K. However, with MW radiation, completion of the reaction can be achieved in a short time and at a much lower temperature, that is, from 673 to 1073 K.[142] Norman and Cha *et al.*[143] reported the activation of char for the synthesis of microporous activated carbon. MW heating has also been used for removing functionalities or reduction of activated carbon. There are other processes that have been simplified and shortened by applying MW heating such as the vulcanization of rubber, MW-assisted polyol process, and drying of carbon xerogels. There are several reports on the use of MW heating for inducing pyrolysis with a carbon mixture and various metal oxides.[77,129–132,144–146] Thus, the MW absorption property of carbon materials makes their synthesis and modification much simpler compared to conventional thermal heating methods.

3.2. Metal oxide nanomaterials

MW heating is also becoming popular for synthesis in areas such as inorganic, organic, and polymer chemistry and biochemical processes. MW radiation has been successfully used for the synthesis of metal nanoparticles with different shapes, sizes, morphologies, and compositions. The nature of nanoparticles is highly dependent on their physical and structural characteristics. Many processes such as solvothermal synthesis, template-assisted synthesis, and thermolysis of precursors have been used for the synthesis of metal nanoparticles.[147–149] The use of MW heating in these syntheses provides a way for the large-scale production and controlling the size of nanoparticles. MWI decreases the activation energy of a reaction with an increase in the reaction rate. The high internal energy results in the fast decomposition of the precursor and fast nucleation growth, resulting in homogeneous morphological and controlled compositional changes in nanoparticles. MW heating also controls the critical size of particles *via* uniform heating rates. Diverse dimensional nanoparticles have been fabricated by controlling the heating time of the reaction and using suitable solvents.[150–157]

The size and morphology of nanoparticles are affected by the growth and nucleation processes. These mechanisms are described by the classical nucleation theory for the growth and nucleation of nanoparticles.[158–160] Nucleation can be of two types, namely, homogeneous nucleation and heterogeneous nucleation. In the case of homogeneous nucleation, no other particles are necessary and the precursor material itself forms a cluster for nucleation. However, for heterogeneous nucleation, the presence of foreign particles is required for the nucleation and growth of nanoparticles. The growth of nanoparticles eventually gives rise to the formation of nanocrystals. This can be summarized in three steps, *i.e.*, nucleation, growth and completion of growth, which is commonly known as Ostwald ripening. In Ostwald ripening two processes occur, which are growth and diffusion limited aggregation and are mainly dependent on temperature. MWI offers constant temperature throughout the solution/material due to fast heating rate and inward heating.

Researchers have synthesized metal ferrite (MFe_2O_3, M = Fe, Mn, Co, Ni, and Zn) *via* the assistance of MWI.[161] In this process, in addition to precursor materials, oleic acid and oleylamine were used as ligating solvents. The results showed a change in morphology by changing the MWI time and also by making some compositional changes. Fig. 6 presents the effect of MWI duration on the morphology of Fe_2O_3. Bilecka *et al.*[162] reported the MW-assisted synthesis of ZnO nanoparticles. The synthesis of ZnO involves esterification and is a first order reaction. The rate constant of the reaction was calculated to be significantly high in case of MW heating (15 nm^3 min^{-1}) in comparison to conventional heating (3.9 nm^3 min^{-1}). These results give clear evidence of the effective heating by MW. Another report on the synthesis of ZnO oxide showed morphological changes with a change in the MWI heating time. It was found under similar conditions, heating for 30 s resulted in the formation of cube-shaped nanoparticles, whereas heating for 60 s resulted in the formation of ZnO nanorods,[67] as shown in Fig. 7.
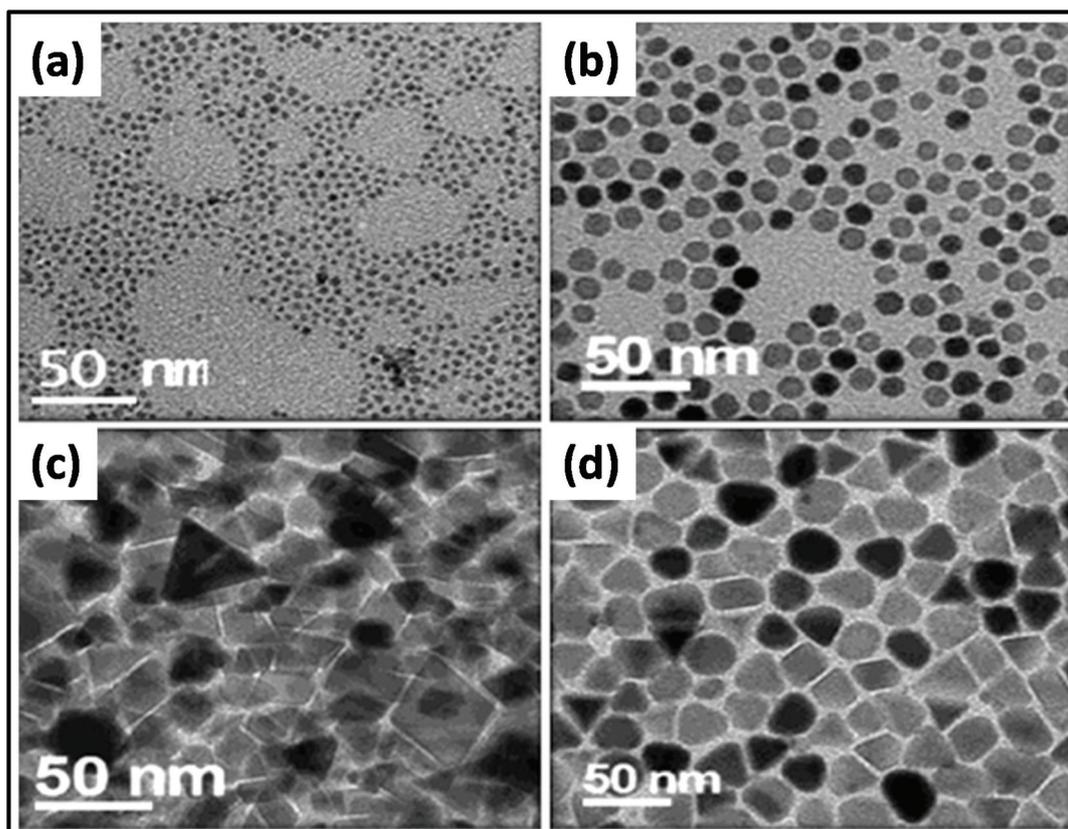
Fig. 6 TEM images of Fe_3O_4: effect of using different compositions and times of MWI. (a) 4 nm and (b) 20 nm prepared using the same ratio of oleic acid to oleylamine (1 : 1) at different MW times (6–8 min and 15–18 min, respectively). (c) Triangular and prism shapes and (d) quasi cubes and triangular shapes prepared using oleic acid to oleylamine ratios of 2 : 1 and 3 : 1, respectively.[161] Reprinted (adapted) with permission from ref. 161, copyright (2013), Springer. All rights reserved.
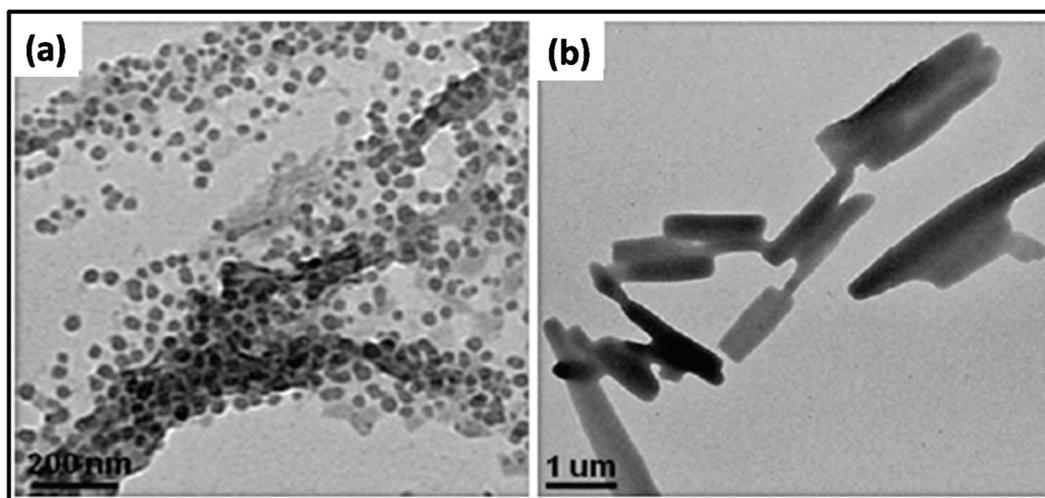
Fig. 7 TEM images of ZnO nanostructures prepared by MWI of 0.1 M zinc acetate solution in pure oleic acid for 30 s (a) and 60 s (b).[161] Reprinted (adapted) with permission from ref. 161, copyright (2013), Springer. All rights reserved.

MW-assisted methods for the synthesis of other metal oxides such as TiO_2, CeO_2, and rare earth oxides (M_2O_3, M = Pr, Nd, Sm, Gd, Tb, and Dy) have also been reported.[163–165] These metal oxides were further used in many applications such as optical communication, oxidation of heavy metal oils, and UV shielding. Transition metal oxides are extensively used in energy storage applications. The MW-assisted synthesis of these metal oxides makes the process cost efficient and easy.

Huang *et al.*[166] developed α-MnO$_2$ nanofibers using an MW-assisted hydrothermal method. This synthesis was performed at 200 °C temperature with a holding time of 10 s–30 min. MnO$_2$ exists in the α, β, γ and δ phases. Chen *et al.*[167] synthesized all the phases of MnO$_2$ *via* MW-assisted synthesis utilizing the reduction reaction of MnCl$_2$-KMnO$_4$ under MWI. There are other reports on the MW-assisted synthesis of different metal oxides such as Co$_3$O$_4$ [168,169] and NiO.[170] TiO$_2$ materials were prepared *via* both conventional and MW heating, in which MW-assisted synthesis resulted in higher crystallinity in a shorter processing time. The MW-assisted synthesis was completed in 30–60 min, whereas conventional heating took 8–12 h for completion.[171]

3.3. Metal hydroxide nanomaterials

Metal hydroxides have also been synthesized *via* MWI and used in many energy storage applications such as rechargeable batteries and supercapacitors.[172–180] The synthesis time and cost are very important for the commercialization of materials, which can both be efficiently improved by MW heating. Xu *et al.*[178] studied the hydrothermal synthesis of 3D flowerlike α-Ni(OH)$_2$ *via* MW-assisted and conventional heating. The XRD pattern of the product, as shown in Fig. 8a, reveals highly intense peaks in the case of MW-assisted synthesis compared to conventional heating. MW heating is more beneficial for the crystalline structure of materials compared to conventional heating. Also, a morphological study showed that particles prepared *via* the MW-assisted method were uniform in shape and size, which was not in the case of conventional synthesis. This uniformity in the shape and size of particles is due to the uniform and rapid heating by MWs. One group described the preparation of α-Ni(OH)$_2$ employing MW heating.[179] Ni(NO$_3$)$_2$·6H$_2$O was used as a precursor in ethanol solvent and heated at 150 °C for 15 min. This green product α-Ni(OH)$_2$ was further transformed into NiO *via* calcination at 300 °C, 350 °C,

and 400 °C. The growth mechanism for the formation of α-Ni(OH)$_2$ followed the same steps as discussed previously for metal oxides. Briefly, nucleation occurs when Ni^{2+} ions are reduced with ethanol in the presence of MW heating. Once α-Ni(OH)$_2$ nucleation occurs, then its growth is dominated by the Ostwald ripening phenomenon. The morphology of α-Ni(OH)$_2$ is dominated by 2D layers, which further grow and give rise to a flower-type morphology.[179] The SEM and TEM images of the synthesized α-Ni(OH)$_2$ are shown in Fig. 8b and c, respectively. The calcined product NiO showed very good cyclic stability and a specific capacitance of 277 F g^{-1}.[179]

The growth of α-Ni(OH)$_2$ using MW-assisted synthesis was also demonstrated by Zhu *et al.*[172] The specific capacitance of α-Ni(OH)$_2$ was 4172.5 F g^{-1} at a current density of 1 A g^{-1}. Besides Ni(OH)$_2$, there are many other transition metal hydroxides that have been synthesized by MW heating. For example, Liu *et al.*[180] synthesized layered cobalt hydroxide nanocones intercalated with dodecylsulphate (DS) ions. The product showed a nanocone-type morphology, in which the size of the tip diameter was 20 nm and the bottom diameter was 400 nm with the length of the cone of 2 μm. For 10 min heating at 100 °C, a mixed morphology of nanocones and sheets was obtained, but on increasing the holding time to 30 min, only nanocones were formed.[180] Some groups also discussed the formation of composites of two metal hydroxides such as Zn–Al double layered structure and composite of Co$_x$Ni$_{1-x}$(OH)$_2$ nanosheets. Chen *et al.*[181] fabricated nanosheets of Co–Ni hydroxide using MW, applying 40% of the maximum power of 1250 W for 3 min, resulting in the composition of Co$_{0.2}$Ni$_{0.8}$(OH)$_2$ having a hexagonal nanosheet morphology. A comparative study was also performed to determine the effect of conventional heating and MW heating on the synthesis of a Zn–Al SDS composite. The results confirmed that MW heating is much faster than the conventional method and endows the material with good crystallinity.[182]
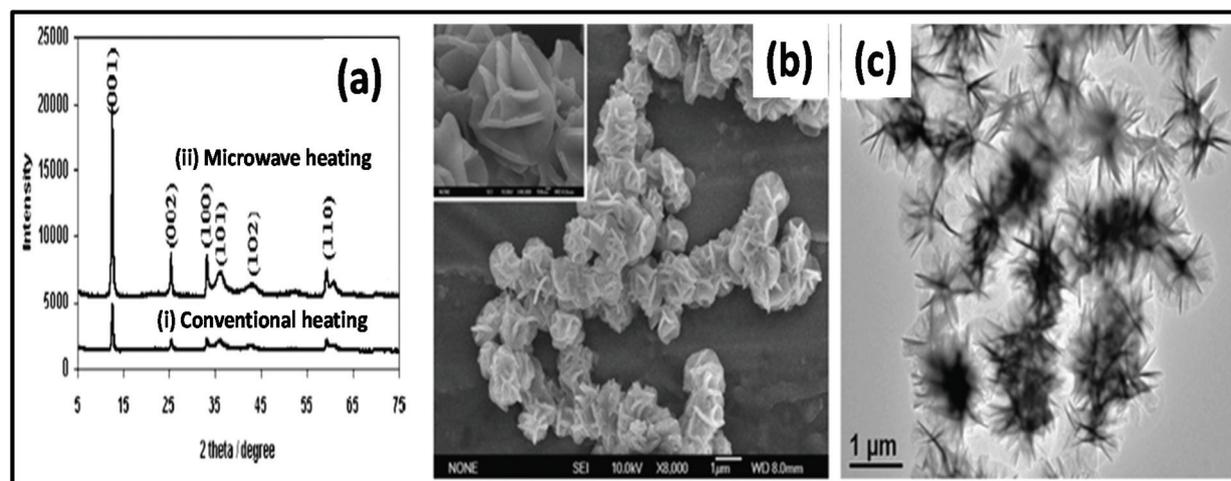

Fig. 8 (a) XRD pattern of α-Ni(OH)$_2$ synthesized by (i) conventional heating method and (ii) MW heating method.[178] (b) SEM image of α-Ni(OH)$_2$ and (c) TEM image of α-Ni(OH)$_2$.[179] Reprinted (adapted) with permission from ref. 178 and 179, copyright (2008 and 2010), the American Chemical Society.

3.4. Carbon mixed metal oxide/hydroxide nanomaterials

It is known that carbon materials contain good MW absorption capacity and many carbon allotropes and nanostructures are used in many applications.[183,184] Thus, the MW-assisted formation of composites can improve the synthesis process, form homogeneous composites and enhance the material efficiency. Composites of carbon and metal oxides/hydroxides have been significantly used in energy storage such as supercapacitors and batteries.[185–196] In conventional heating, the synthesis mechanisms commonly lead to heterogeneous nucleation due to the temperature gradient. However, in MW-assisted synthesis, carbon materials mostly act as a substrate given that they have good absorption capacity toward MWs. Also, the presence of carbon materials and the concentration of the precursor materials considerably affect the morphological-dependent characteristics. Kim et al.[197] studied the morphology of an rGO and Co/Ni(G/CoNi) hydroxide composite. It was deduced that with a change in the composition of CoNi, the morphology of the product changes. For the compositional ratio of 4 : 1 (G/CoNi), a sheet-like morphology was formed, whereas for 1 : 4 ratio, aggregation of the CoNi particles occurred, which resulted in the formation of a nanosphere-type of morphology. The advantage associated with MW-assisted synthesis is that the reduction of graphite oxide and the formation of the composite occur simultaneously. The composite also gave a superior electrochemical performance with a specific capacitance of 1622 F g^{-1} for G-CoNi 2 : 1.[197] Fig. 9 reveals the effect of MWI time on the morphology of multi-walled CNT (MWCNT)/Ag nanoparticles. The diameter of Ag nanoparticles varies with a variation in the MW irradiation time. Composites were prepared by mixing silver acetate as a silver source and MWCNT powder in a stoichiometric ratio using a mortar and pestle. This mixture was then irradiated for 60 min at the power of 300 W and temperature of ~300 °C. A similar study was conducted using conventional heating methods, in which the average diameter of the nanoparticle was 40–50 nm. However, in the case of the MW-assisted synthesis, the average diameter of the nanomaterial was much larger, i.e., 20–100 nm.[198] Loupy et al.[199] revealed that MW-assisted synthesis produced a 90% increase in yield compared with conventional synthesis. Several studies confirmed that the increase in yield is purely because of non-thermal MW effects. Numerous studies have demonstrated the formation of CNTs and metal hydroxide and metal oxide composites.[200,201]

A CNT/RuO$_2$ composite was obtained by Kim et al.,[202,203] in which the uniform distribution and loading of nanoparticles on CNT was achieved by controlled heating. Up to 70% loading of RuO$_2$ with an average diameter of 2 nm was achieved. Guo et al.[204] prepared uniform carbon-coated ZnO nanorods via MW-assisted synthesis and studied their photocatalytic activity cytotoxicity. Prior to MWI, the surface of the ZnO rods was modified by amino groups. The system was then irradiated at 100 °C for 30 min, resulting in the formation of the composite. The TEM and SEM images of the samples revealed that rods were uniform with an average size of ~12 nm. The particle size distribution is shown in the inset of the graph in Fig. 10a.

3.5. Current state of the art on microwave-assisted synthesis: carbon nanomaterials and metal oxide/hydroxide nanomaterials

The current trend of MW synthesis is mainly focused on the development of advanced carbon materials with high porosity, enhanced surface area, and superior mechanical properties. Nano-structured carbon materials are significantly synthesized using various MW routes including MW-assisted pyrolysis, MW-induced hydrothermal/solvothermal process, and MW-assisted activation.[205] In a recent study, N-doped and oxygen-functionalized carbon nanoonions were combined with Pd nanoparticles through MW heating.[206] The resultant composite was utilized as an efficient anode electrocatalyst for alkaline fuel cells. In another report, Eskalen et al. demonstrated the MW-assisted hydrothermal synthesis of carbon dots from acid linter waste.[207] The carbon dots displayed efficiency for fluorescence cancer imaging and human cell growth inhibition properties. Moreover, carbon quantum dots were synthesized using citric acid and urea in a domestic MW oven.[208] A dark brown cluster of carbon quantum dots was prepared within a period of 300 s. A pictorial overview of the color change in the intermediates of this MW synthetic route is shown in Fig. 11. This special type of carbon material displayed enhanced optical properties, which can be efficient for organic solar cells.

The MW-assisted synthesis process was further extended to the synthesis of N,S-doped carbon dots using citric acid and thiourea.[209] With the MW power of 550 W, the doped carbon nanomaterial was synthesized within only 5 min, indicating a rapid and efficient synthetic route. The doped carbon dots demonstrated extensive mercury ion sensing properties. In a recent study, Xia et al. demonstrated the ultrafast MW-assisted synthesis of N-doped mesoporous carbon on Ni foam.[210] A strong MW power of 1000–2000 W was applied to melamine-loaded resol-coated Ni foam under an N$_2$ atmosphere for only 3 min to synthesize this special type of carbon material. The MW heating process was further implemented to produce a composite of histidine-functionalized graphene quantum dots and Ni–Co layered double hydroxide (LDH).[211] The composite displayed superior electrochemical performances, and thus can be applied in the fabrication of supercapacitor electrodes. MW synthesis route has also been found to be beneficial for the development of other supercapacitor electrodes. For example, graphene was combined with MoS$_2$ through MW heating using sodium molybdate dihydrate (Na$_2$MoO$_4$·2H$_2$O) as the Mo precursor and L-cysteine as the sulfur source and reducing agent.[212] Besides graphene, CNT was also combined with a metal oxide such as NiO through MWI at a high power of 560 W for 10 min in a domestic MW oven.[213] The current MW reaction process was successful with the assistance of H$_2$O$_2$. Similar to the previous report, the current composite also demonstrated excellent electrochemical performances for application in supercapacitors. All these studies clearly indi-
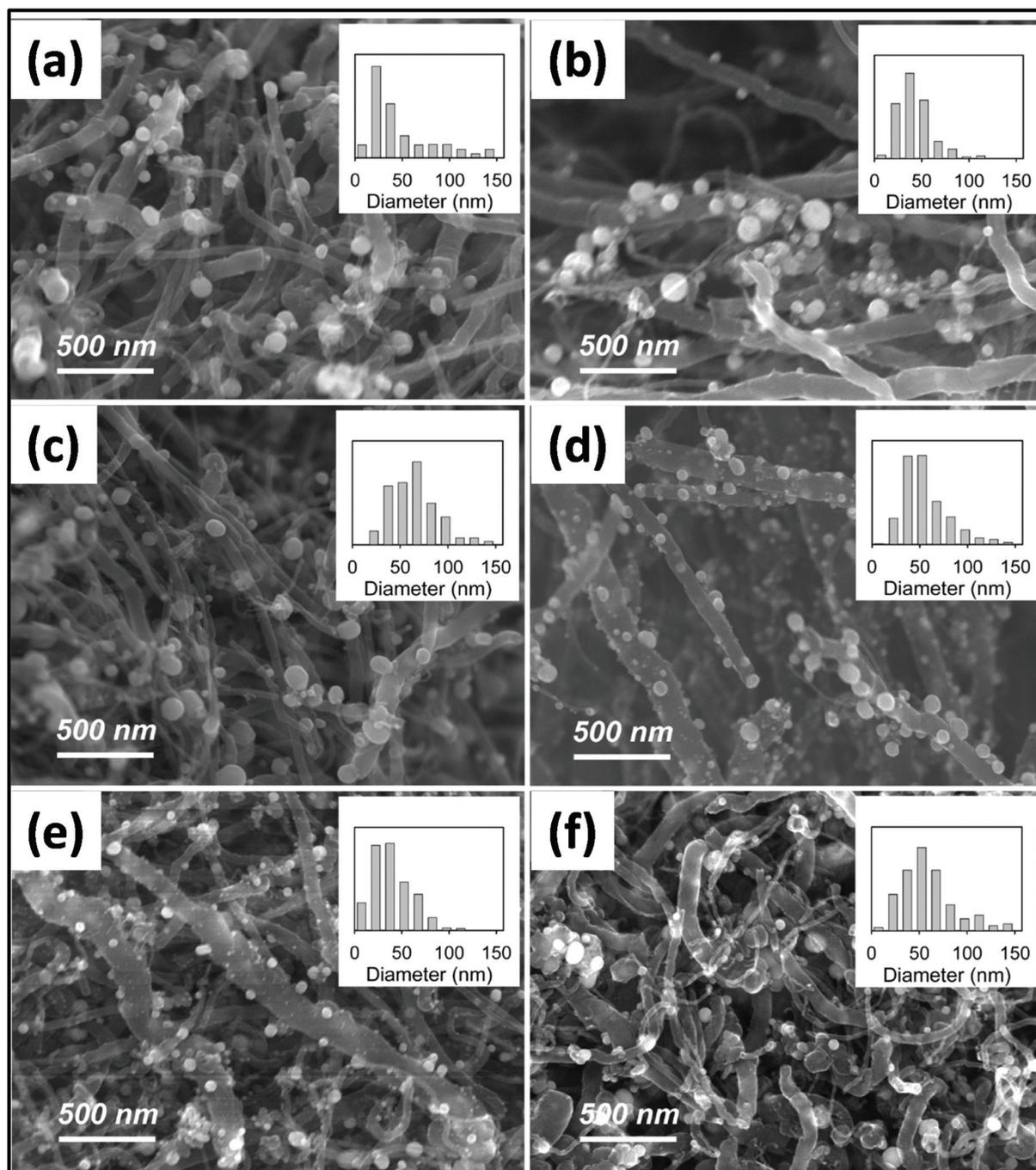
Fig. 9 SEM images of various samples of silver/MWCNT starting material (a) 1 min, (b) 2 min, (c) 5 min, (d) 10 min, (e) 30 min, and (f) 60 min, of MWI.[198] Reprinted (adapted) with permission from ref. 198, copyright (2011), the American Chemical Society.

cate the impact of the MW synthetic route for producing nano-structured carbon materials with versatile application potential.

The MW synthetic route has been considered an eco-friendly, green, and sustainable synthetic approach for the production of metal oxides with nano-architectures. In recent years, MW heating was found to be more beneficial compared to the conventional heating approach in terms of reaction time

and product yield.[214] For example, the MW-assisted hydro-thermal approach was employed by Zhang *et al.* to synthesize beta-bismuth(III) oxide (β-Bi_2O_3) nanopowder.[215] The synthetic approach was successful in reducing the reaction time from 24 h to 2 h. The resultant metal oxide demonstrated superior photocatalytic properties for the degradation of methyl orange. Mixed metal oxides are a new class of metal oxides, which are suitable for many future applications. In this case,
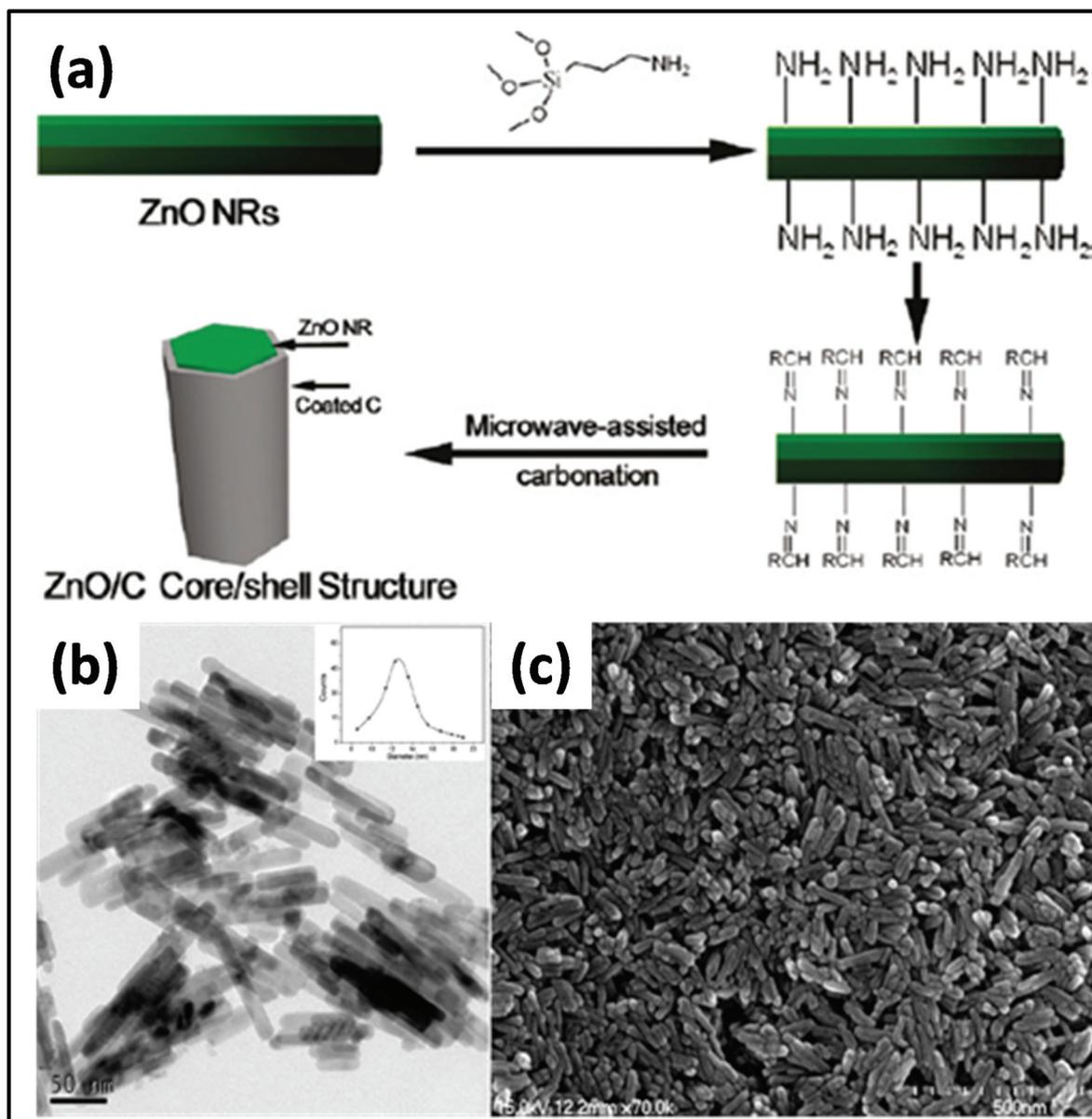
Fig. 10 (a) Schematic diagram showing the synthesis of carbon-coated ZnO. (b) TEM (inset: average size distribution of 200 rods) and (c) SEM images of ZnO nanorods.[204] Reprinted (adapted) with permission from ref. 204, copyright (2009), the American Chemical Society.

Hashemzehi *et al.* reported a MW-assisted solution combustion process to produce a Cu–Zn–Al mixed metal oxide.[216] In another report, a Ti/(RuO$_2$)$_{0.5}$(IrO$_2$)$_{0.5}$ anode was synthesized through an MW heating process at a high MW power of 700 W for application in the dye degradation process.[217] A comparative study on the dye degradation properties of the mixed metal oxide synthesized *via* conventional and MW heating clearly indicated the superior performance of the MW-synthesized metal oxide. Moreover, a CoMnMgAl mixed oxide catalyst was synthesized through an MW-assisted self-combustion process.[218] The mixed metal oxide exhibited promising catalytic activity for the total oxidation of toluene. For sensing applications, MW technology has also been employed. For

example, a CuO/ZnO heterojunction composite was synthesized through an MW-epoxy-assisted hydrothermal method.[219] This composite demonstrated promising H$_2$S gas sensing properties. To understand the MW synthetic approach, the synthesis process of this metal oxide-based composite is schematically shown in Fig. 12. In another report, a nanocomposite based on CdO and MgO was synthesized through an MW-assisted green approach using the acetate precursors of Cd and Mg.[220] This composite displayed excellent antimicrobial, anti-breast and anti-lung cancer activity. Superior antibacterial activity was further exhibited by (Ag, Co)-codoped CuO nanoparticles, which were synthesized through the MWI approach.[221] In a typical process, all the precursor materials
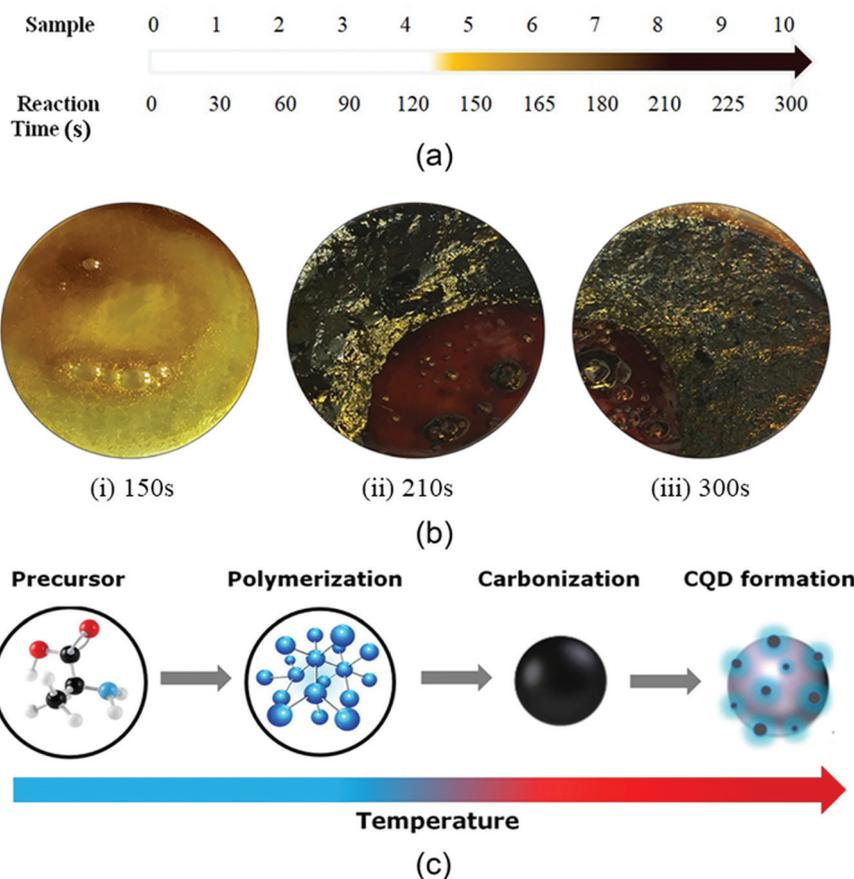
Fig. 11 (a) Change in sample color with reaction time. (b) Samples depicting the change in color and CQD formation upon heat treatment of (i) 150 s, (ii) 210 s, and (iii) 300 s. (c) Reaction pathway for the synthesis of CQDs with an increase in temperature.[208] Reprinted (adapted) with permission from ref. 208, copyright (2020), Taylor & Francis Group. All rights reserved.

were irradiated with the MW energy of 2.45 GHz at the corresponding power of 800 W for 30 min.

For further property enhancement, metal oxides have been combined with carbon nanomaterials through the MWI process. For example, in a recent study, Kumar *et al.* proposed a MWI approach for the synthesis of an Mn_3O_4-Fe_2O_3/Fe_3O_4@rGO ternary hybrid for the fabrication of advanced supercapacitor electrodes.[222] Using graphite oxide as the precursor for graphene, the authors applied a high MWI power (900 W) for only 30 s to achieve the ternary hybrid. It is important to mention that the consecutive exfoliation and reduction of graphite oxide to form graphene are possible through MWI. A schematic of the synthetic approach and the mechanism of the synthesis of the ternary hybrid are presented in Fig. 13.

A MW-induced hydrothermal process was employed to synthesize a ternary nanocomposite based on Fe_3O_4, rGO, and MoO_3 for energy storage application.[223] In the presence of MWI, the hydrothermal reaction time was restricted to only 1 h. Table 3 provides a summary of the various works based on the MW-assisted synthesis of metal oxides, metal hydroxides, and composites of carbon materials/metal oxides/hydroxides and their related applications.

4.   Recent trends on microwave-assisted hydrothermal/solvothermal synthesis of organic nanomaterials

Similar to other synthetic areas, MW heating is significant in solvent-mediated hydrothermal/solvothermal organic synthesis. MW-assisted organic synthesis can be done using water or other polar solvents. Many organic reactants are insoluble in water, which results in an inhomogeneous solution. However, MW heating relies on dielectric heating, and thus the behavior of a particular solvent changes with a change in temperature due to the change in dielectric constant. The dielectric constant of water is 78 at 25 °C and 20 at 300 °C, respectively. Thus, at high temperature, water can act as a pseudo-organic solvent for many organic syntheses. MW heating also makes solvent-free synthesis feasible.[76,245,246] Organic synthesis proceeding in water and other solvents is heavily applied in industrial applications.

4.1.   Hydrolysis of benzyl alcohol and benzamide

These reactions usually take approximately 35 min and 1 h for the hydrolysis of benzyl chloride and benzamide, respectively.
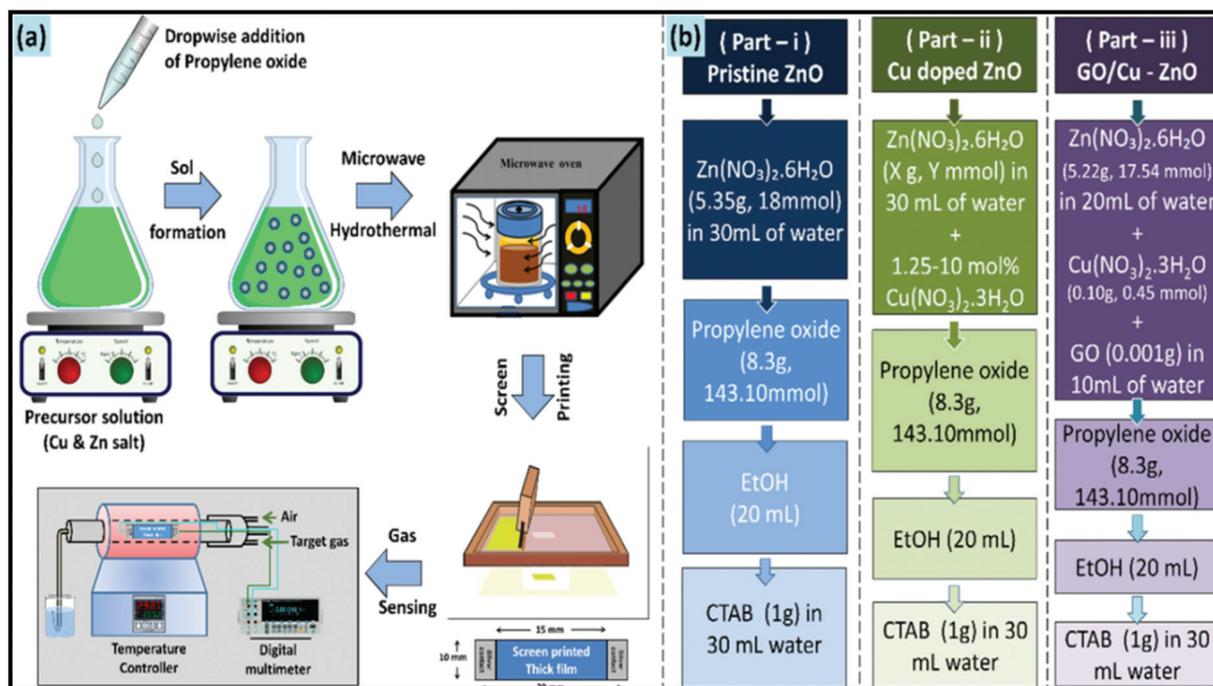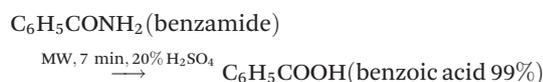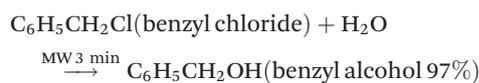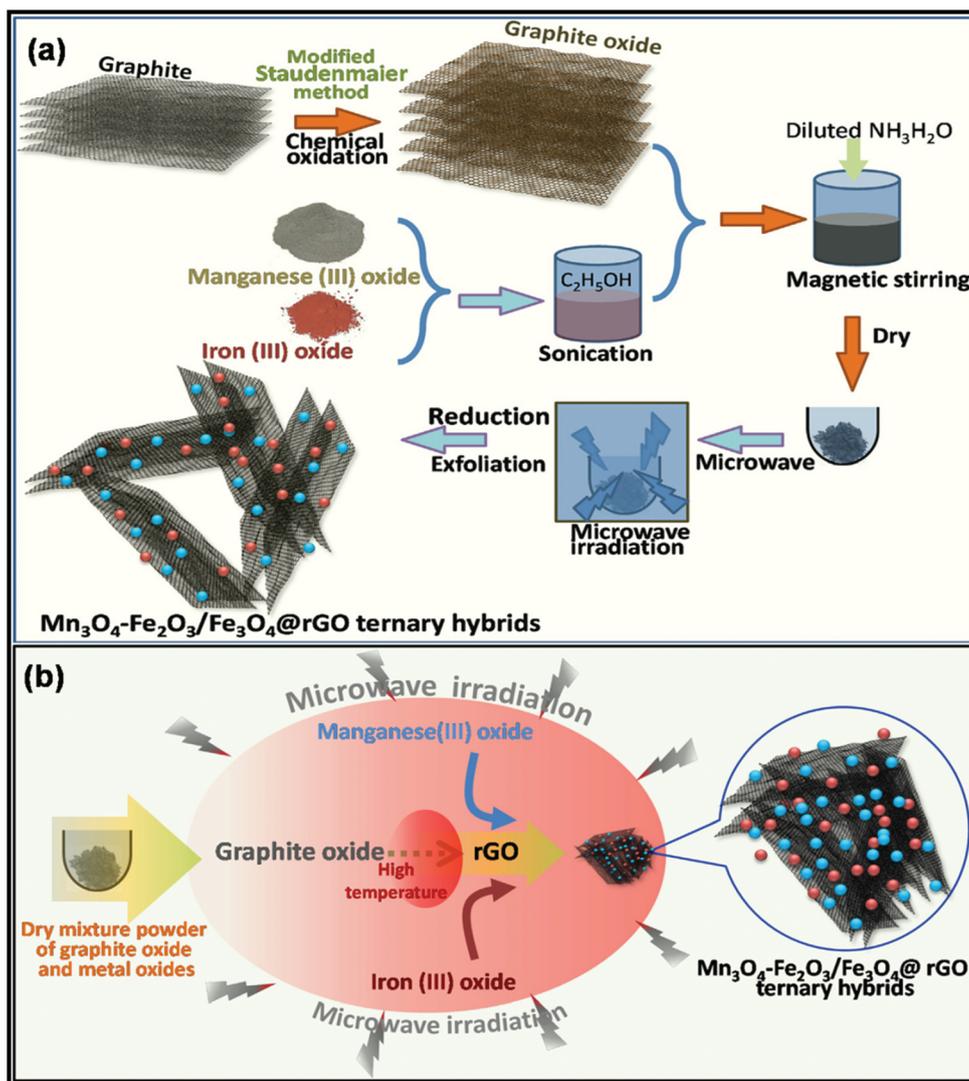
Fig. 13 Schematic presentation of the (a) synthesis process and (b) mechanism of MW-assisted formation of Mn_3O_4-Fe_2O_3/Fe_3O_4@rGO ternary hybrid.[222] Reprinted (adapted) with permission from ref. 222, copyright (2020), Elsevier B.V. All rights reserved.

energy-related applications such as supercapacitors and batteries.

4.4. Supercapacitors

Metal and metal oxide/hydroxide nanoparticles have been used for supercapacitor applications as electrode materials. Zhang *et al.*[257] synthesized γ-MnO_2 and α-MnO_2 using MWI in 5–30 min. The morphology results showed that as the radiation holding time increased, the morphology of MnO_2 was affected. With an increase in MWI time from 5 min to 30 min, the number of nanowires and nanoplatelets increased together with an increase in their length, as shown in Fig. 15. Fig. 15a–f correspond to the synthesis in acidic conditions and Fig. 15g–l correspond to the synthesis in neutral conditions at different MW heating times. In acidic conditions, an urchin-like nanostructure morphology was formed, which consisted of uniform nanorods. In the neutral case, the MnO_2 showed a nanoplate-

let and nanowire morphology. This indicates that the experimental conditions significantly affect the products. The highest specific capacitance offered by MnO_2 was 311 F g^{-1} at a current density of 0.2 A g^{-1}, which was obtained for γ-MnO_2 nanoparticles. Thus, this method provides a way that is much more cost efficient and less time consuming compared to the conventional synthesis method. Also, this provides a way of controlling morphological aspects by controlling the heating time.[257] Co_3O_4 was synthesized using MW heating at 240 W for 5 min. $Co(NO_3)_2\cdot6H_2O$ was used as the cobalt source and water and ammonia were used as the solvent and for maintaining the pH of the solution, respectively. After MW treatment, the precipitates were calcined at 300 °C for 1 h. The size of the nanoparticles was found to be uniform and the mean particle size was 24 nm. The uniform size of the nanoparticles was due to the uniform heating by MWI. Electrochemical measurements of these nanoparticles gave the maximum specific

Table 3 Summary of some of the published reports on the MW-assisted synthesis of metal oxides, metal hydroxides, and composites of carbon materials/metal oxides/hydroxides and their applications

Material	Material type	Precursors/solvent	Morphology and structure of materials	MW condition	Results/application	Ref.
Metal oxide	MgO, NiO, ZnO, ZrO$_2$, Fe$_2$O$_3$, Al$_2$O$_3$	Magnesium ethylate, zinc acetate tetrahydrate, nickel acetate tetrahydrate, aluminium-tri-*sec*-butoxide, ferric acetate, zirconium(IV) isopropoxide/ethyl acetate, ethanol, PVP	Amorphous powder with particle size in the range of 0.7–3.7 nm after annealing.	30 min	Nanoparticles prepared by MW-assisted synthesis	224
	Bi$_2$O$_3$	Bi(NO$_3$)$_3$·5H$_2$O, nitric acid/H$_2$O	Nanorods	6 min refluxing at medium power of MW oven	Cost effective for synthesis of Bi$_2$O$_3$ nanorods	225
		PVP, NaOH	Diameter ~100 nm; length: several micrometers/monoclinic crystalline α-Bi$_2$O$_3$			
	CeO$_2$	(Ce(NO$_3$)$_3$·6H$_2$O), HAuCl$_4$·4H$_2$O, sodium hydroxide/urea, ammonia, and ethanol	14 nm spheres assembled in hollow spheres (260 nm)	170 °C for 30 min	Good absorption capacity for heavy metal ions	226
	Co$_3$O$_4$	Cobalt nitrate and urea	Foamy porous morphology with cubic spinel structure.	15 min at 2.45 GHz, 800 W.	Coercivity value was 56.7 Oe.	227
	CuO	Cu(CH$_3$COO)$_2$/EtOH NaOH, PEG	Sphere morphology with average size of 4 nm and single-phase monoclinic CuO	10 min heating with 20 MW heating cycles (6 s ON/24 s OFF)	Band gap estimated to be 2.43 eV	228
	α-Fe$_2$O$_3$	FeCl$_3$·6H$_2$O/HCl	Spheres 31–66 nm with α-Fe$_2$O$_3$	2–8 h	Effect of MWI on morphology and other aspects affecting characteristics	229
	Cr$_2$O$_3$, MoO$_2$, CoO, Mn$_2$O$_3$	K$_4$Fe(CN)$_6$, K$_3$Co(CN)$_6$, K$_3$Mn(CN)$_6$, K$_3$Mo(CN)$_8$, K$_3$Cr(CN)$_6$/H$_2$O	Octahedral, spherical, rod, pine tree, snowflake-like assemblies 1–5 mm with orthorhombic Mn$_2$O$_3$, cubic Cr$_2$O$_3$, MoO$_2$, CoO structures	100–160 °C 3 h at 180 °C, >1 atm	Obtained nanoparticles can be used for biomedical and catalytic properties	230
	In$_2$O$_3$, Tl$_2$O$_3$	Indium(III) chloride, thallium(III) chloride/NH$_4$OH	Hexagons 22 nm (In$_2$O$_3$) and spherical nano-particles (Tl$_2$O$_3$) with BCC In$_2$O$_3$, and cubic Tl$_2$O$_3$	60 m (MW cycles: 12 s ON/7 s OFF) reflux	BCC structured In$_2$O$_3$ and cubic Tl$_2$O$_3$ were prepared	231
	PdO	PdCl$_2$/H$_2$O, PVP, NaOH NaOAc, C$_6$H$_5$CO$_2$Na	Spheres 1.8–3.2 nm and σ = 25% with FCC structure	8 min refluxing at 900 W with 10% output power	Palladium oxide nanoparticles with FCC structure synthesized	232
	SnO$_2$	SnCl$_4$·5H$_2$O/H$_2$O, urea	SnO$_2$ nanoparticles (size: 3 nm)	15 min refluxing with a 650 W power with 10% output	Optical measurement showed a band gap of 4.5 eV	233
	TiO$_2$	TiCl$_4$, HCl, NH$_4$OH	TiO$_2$ nanorods (diameter: 20–30 nm; length: 150–250 nm)	5 min–8 h, 25–80 °C, 1 atm	Facile approach for synthesis of TiO$_2$	234
	WO$_3$	Na$_2$WO$_4$·2H$_2$O, H$_2$O, (NH$_4$)$_2$SO$_4$, HCl	WO$_3$ nanowires (diameter: 5–10 nm; length: 8–10 μm)	20 min–3 h, 150 °C, >1 atm	High electrocatalytic activity for hydrogen evolution reaction	235
	ZnO	Zn(OAc)$_2$, hydrolyzed in di-ethylene glycol (DEG)	ZnO colloidal nanocrystal clusters (nanocrystal size: 8 nm; cluster size: 57 to 274 nm)	1–5 min steps, 120–180 °C, 1 atm	Highly sensitive sensor for sensing humidity	236
	ZrO$_2$	ZrOCl$_2$·8H$_2$O/NaOH	Spheres 10–20 nm with monoclinic structure	120 min at 194 °C at 14 atm	Nanosized and crystalline particles of ZrO$_2$ were obtained	237
Metal hydroxide	α-Ni(OH)$_2$	Ni(NO$_3$)$_3$·6H$_2$O/EtOH, urea	3D flower-like morphology with size of 700 nm–1 mm and it is α-Ni(OH)$_2$ single phase	90 °C for 15 min	Enhanced electrochemical activity due to flower-like morphology	178
	Mg(OH)$_2$	Mg(NO$_3$)$_2$/H$_2$O, NaOH	Fibre like 20–40 nm, 100–150 nm with a hexagonal phase	4 days under MW (20 W) at 25 °C	Fibre-like Mg(OH)$_2$ was synthesized	238

Table 3 (Contd.)

Material	Material type	Precursors/solvent	Morphology and structure of materials	MW condition	Results/application	Ref.
Carbon	rGO-ZnO	$Zn(AC)_2 \cdot 2H_2O$, RGO sheets	ZnO nanocrystals are anchored on wrinkly rGO sheets,[239] ZnO nanorods apparently originate from a centre forming flower-like morphologies distributed on the surface of rGO[240]	300 W for 10 min,[239] MW treatment for 30 min[240]	Photoactivity for the decolorization of dyes under visible light,[239] adsorption-photocatalysis[240]	239 and 240
	GQDs-CuO nanoneedles	Cupric acetate, GO/NaOH, H_2O, H_2O_2	GQDs/CuO nanocomposite has a spindle-shaped structure of 80 ± 10 nm in length and 16 ± 5 nm in width and structure of CuO is monoclinic	Under 800 W at 200 °C for 8 min	For the sensing of the H_2O_2 and glucose	149
	Graphene-CuO	Cupric acetate, GO/DMF	Quasi-spherical CuO nanoparticles embedded on graphene sheets, 30–50 nm in size with CuO monoclinic crystal structure	800 W for 20 min	For the detection of bisphenol-A	241
	CNT-RuO$_2$	$RuCl_3$, CNT/H_2O and NH_3	Average diameters of RuO_2 nanoparticles 1–2 nm	~700 W for 30 s	For electrochemical supercapacitors	242
	CNT-MnO$_2$	$KMnO_4$, CNT, nitric acid	MnO_2 can be rapidly nucleated on the wall of CNTs	10 min MWI at 700 W	Specific capacitance based on MnO_2 was 944 and 522 F g^{-1} at 1 and 500 mV s^{-1}	243
	Graphene/hierarchy structure MnO$_2$	$KMnO_4$, $MnSO_4 \cdot H_2O$, GO/H_2O	MnO_2 nanospheres with a size in the range of 100 to 200 nm uniformly distributed on graphene sheet and structure of MnO_2 is birnessite type.	75 °C for 30 min (the controlled power was approximately 450 W)	Specific capacitance of 244 F g^{-1} at a current density of 100 mA g^{-1}	167
	NiAl-layered double hydroxide/rGO	$Ni(NO_3)_2 \cdot 6H_2O$, $Al(NO_3)_3 \cdot 9H_2O$ and GO	NiAl-LDH nanosheets are attached to the surface of rGO and structure of NiAl-LDHs is hexagonal	MWI for 2 h at 100 °C	Specific capacitance of 1630 F g^{-1} at 1 A g^{-1} in 6 M KOH	244

PVP: polyvinylpyrrolidone; DMF: N,N-dimethylmethanamide; PEG: polyethylene glycol; and EtOH: ethanol.

capacitance of 346 F g^{-1} at a scan rate of 5 mV s^{-1}. The specific capacitance was the maximum at a low current density and low scan rates.[258] Wang et al.[259] reported the electrochemical properties of a composite of metal/metal oxide nanoparticles on graphene synthesized via MW-assisted one-pot synthesis. The metal used for the formation of this composite was PtRu and the metal oxide was SnO_2.[259] Fig. 16 shows the cyclic voltammetry (CV) and galvanometric charge/discharge curves for the samples MnO_2-A-5 and MnO_2-N-5, where 5 is the MW holding time and N and A mean neutral and acidic conditions, respectively. It was found from the CV that the entire curve showed a rectangular shape, which did not change much with an increase in the scan rate, indicating that the material has good capacitive reversibility. This good specific behavior was due to the unique morphology of the material. According to the galvanometric charge/discharge curves, the maximum specific capacitance was 311 F g^{-1} at a current density of 0.2A g^{-1} in the case of MnO_2-N-5, which was less than that of MnO_2-A-5 (163 F g^{-1}). This difference was because of the large surface area of MnO_2-N-5, which was 76 m^2 g^{-1}. Another report was published on the MW-assisted synthesis of RuO_2 by Devadas et al.[260] The calculated specific capacitance was 737 F

g^{-1} at a scan rate of 2 A g^{-1}. Kumar et al.[261] also synthesized copper-tungstate nano-powder via MW-assisted synthesis. The nano-powder of Cu-WO_4 showed a specific capacitance of 77 F g^{-1}.[261] There are many reports on different types of nano-materials and their further use for supercapacitors applications such as Mn_3O_4[262] and $NiCo_2O_4$.[263]

Nowadays, researchers are highly focused on the synthesis of electrode materials using MW-assisted methods. The low-cost synthesis of 3D flower-like NiCo microspheres via the MW route without using any template/surfactant under atmospheric pressure for electrode materials in supercapacitors was reported by Li et al.[175] The electrochemical analysis showed that the NiCo electrodes exhibited a specific capacitance of 1120 and 996 F g^{-1} at 1 at 10 A g^{-1}, respectively. After 2000 cycles, the capacitance reached 122.5% of its initial value at 10 A g^{-1} and retained 93.8% at 30 A g^{-1} after another 1000 cycles. The asymmetric supercapacitor with NiCo as the positive electrode and activated carbon from coal as the negative electrode exhibited an energy density of 42.5 W h kg^{-1}. Chandrasekaran et al.[264] reported the MW-assisted synthesis of mesoporous hollow MnCuAl layered triple hydroxide nanocomposites as electrode materials in symmetrical supercapacitors. The Mn–
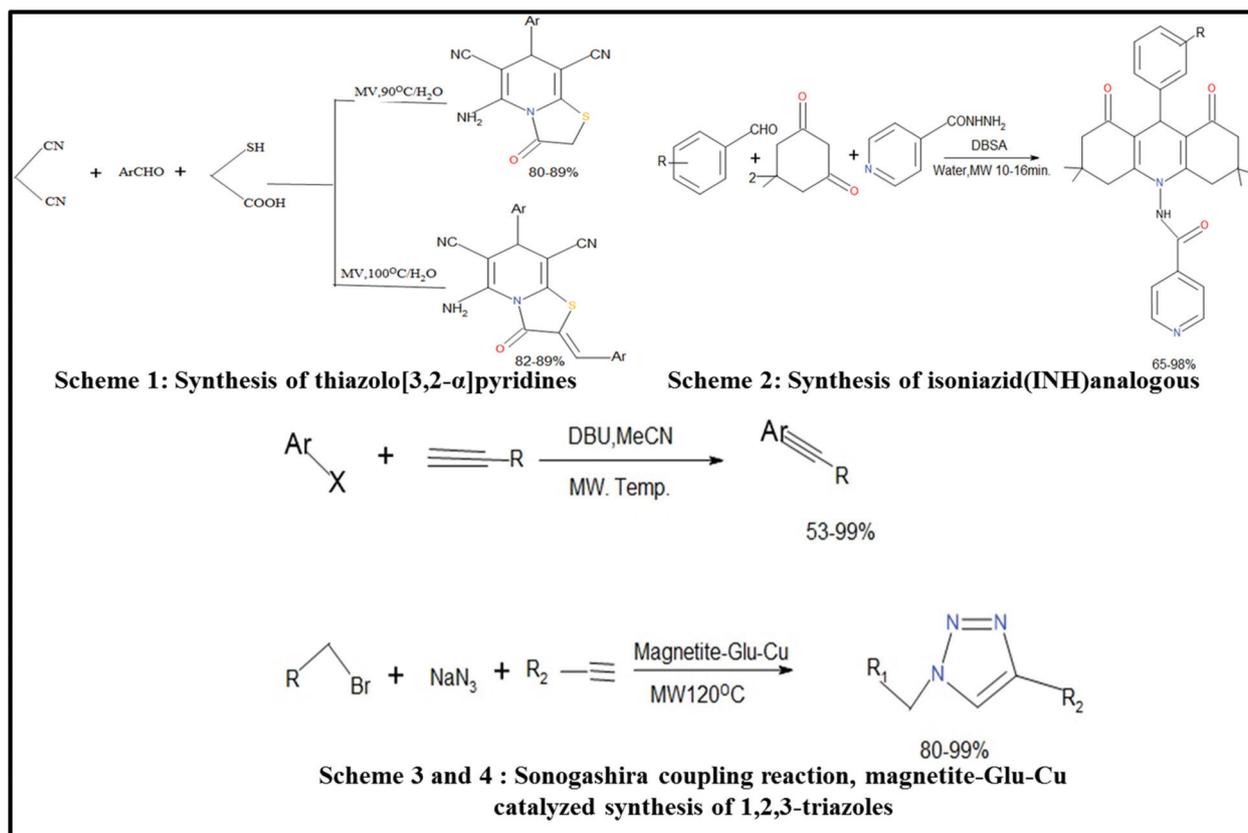
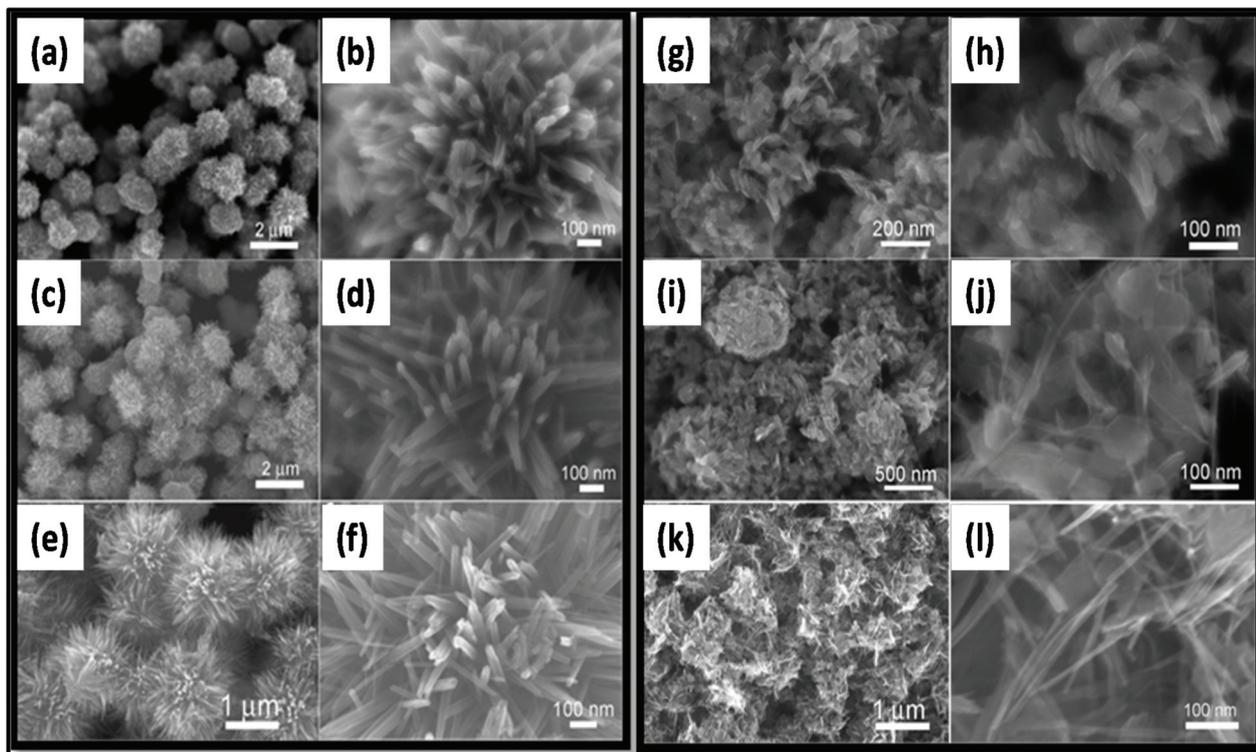**Fig. 14** Scheme for synthesis *via* the MW-assisted method.[76,250–252]

Fig. 15 SEM images of MnO$_2$ prepared at (a, b, g, and h) 5 min, (c, d, i, and j) 10 min, and (e, f, k, and l) 30 min under (a–f) acidic condition and (g–l) neutral condition.[257] Reprinted (adapted) with permission from ref. 257, copyright (2013), Elsevier B.V. All rights reserved.
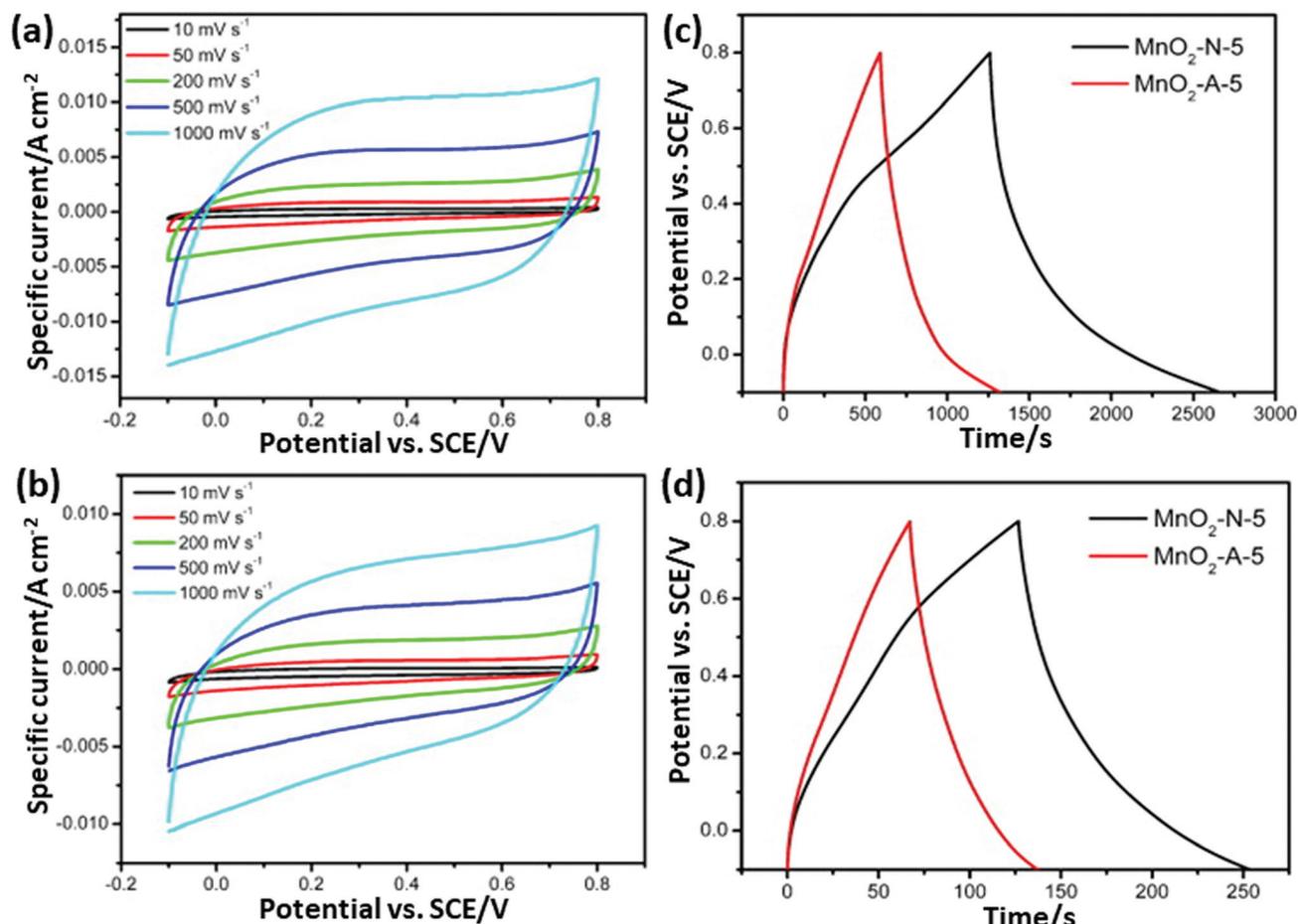
Fig. 16 (a and b) CV curves of MnO_2-N-5 and MnO_2-A-5 at different scan rates and (c and d) charge/discharge curves of MnO_2-N-5 and MnO_2-A-5 at current densities of 0.2 A g^{-1} and 1 A g^{-1}, respectively.[257] Reprinted (adapted) with permission from ref. 257, copyright (2013), Elsevier B.V. All rights reserved.

Cu–Al layered triple hydroxide exhibited 93.46% of its initial capacitance after 5000 cycles. The symmetric solid-state supercapacitor device using Mn–Cu–Al layered triple hydroxide delivered an energy density of 101.75 W h kg^{-1} at a power density of 900 W kg^{-1}. Xia *et al.*[265] demonstrated the MW-assisted synthesis of layered metal hydroxide nanosheet arrays for aqueous hybrid supercapacitors (Fig. 17a). The $Ni(OH)_2$ nanosheets arrays delivered a capacitance of 2516 and 1273 F g^{-1} at 1 and 20 A g^{-1}, respectively (Fig. 17b). The $Ni(OH)_2$//activated carbon aqueous hybrid supercapacitor delivered an energy density up to 66.7 W h kg^{-1} at 400 W kg^{-1} with cycle stability of 85.2% (Fig. 17c and d).

The MW-assisted synthesis of 3D-connected α-$Ni(OH)_2$ sheets as supercapacitor electrode materials was reported by William *et al.*[266] The 3D-connected α-$Ni(OH)_2$ sheet electrodes exhibited a specific capacitance of 549 F g^{-1} at 2 A g^{-1} and capacitance retention of 87.3% even after 10 000 charge/discharge cycles. The supercapacitor device (α-$Ni(OH)_2$/polyurethane foam-6 M KOH/activated carbon) delivered an energy density of 57 W h kg^{-1} at a power density of 601 W kg^{-1}. Fu *et al.*[267] described the MW deposition synthesis of $Ni(OH)_2$/

sorghum stalk biomass carbon electrode materials for supercapacitors. Biomass carbon was synthesized using sorghum stalk as the raw material, and $Ni(OH)_2$ was decorated on the sorghum stalk biomass carbon *via* a MW deposition method, as shown in Fig. 18a. The $Ni(OH)_2$/sorghum stalk biomass carbon exhibited specific capacitances of 889.2 and 490.1 F g^{-1} at a current density of 2 and 20 A g^{-1}, respectively (Fig. 18b). It showed good stability with the capacitance retention of 95.9% over 30 000 cycles at 20 A g^{-1} (Fig. 18c).

The MW-assisted thermal treatment-based synthesis of 3D N-doped graphene coated with ZnO/NiO nanoparticles as electrodes in supercapacitors was suggested by Zhang *et al.*[268] ZnO/NiO nanoparticles with a size in the range of 10–20 nm were anchored on 3D N-doped graphene, which exhibited a specific capacitance of 1839.4 F g^{-1} at a current density of l A g^{-1}. After 6000 charge/discharge cycles at 10 A g^{-1}, the specific capacitance of the ZnO/NiO/3DNG electrode achieved 93% retention of its initial capacitance. The ZnO/NiO/3D N-doped graphene composite exhibited the maximum energy density of 35.32 W h kg^{-1} with the power density 139.72 W kg^{-1} at current density of 10 A g^{-1}. Kim *et al.*[269] described the MW-
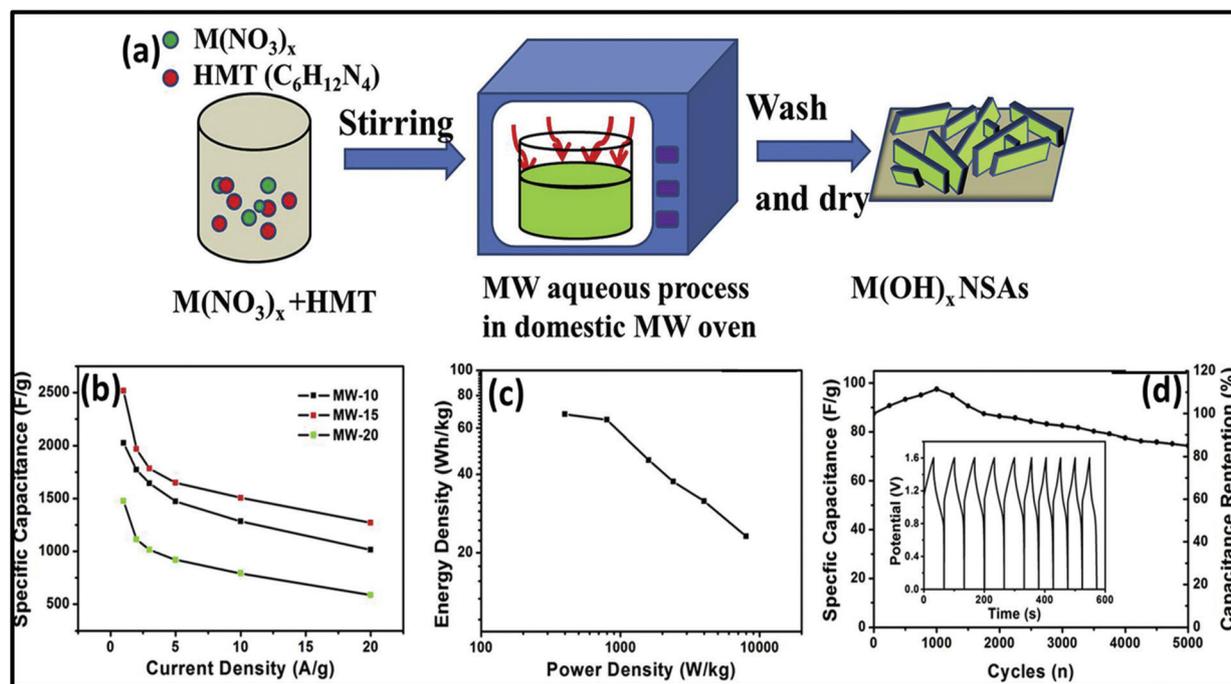
Fig. 17 (a) Schematic of MW-assisted synthesis of layered metal hydroxide nanosheet arrays, (b) specific capacitance *vs.* current density of $Ni(OH)_2$ nanosheet arrays, (c) Ragone plot and (d) cycle curves of $Ni(OH)_2$ nanosheet arrays//activated carbon aqueous hybrid supercapacitor. Reprinted (adapted) with permission from ref. 265, copyright (2019), Elsevier B.V. All rights reserved.
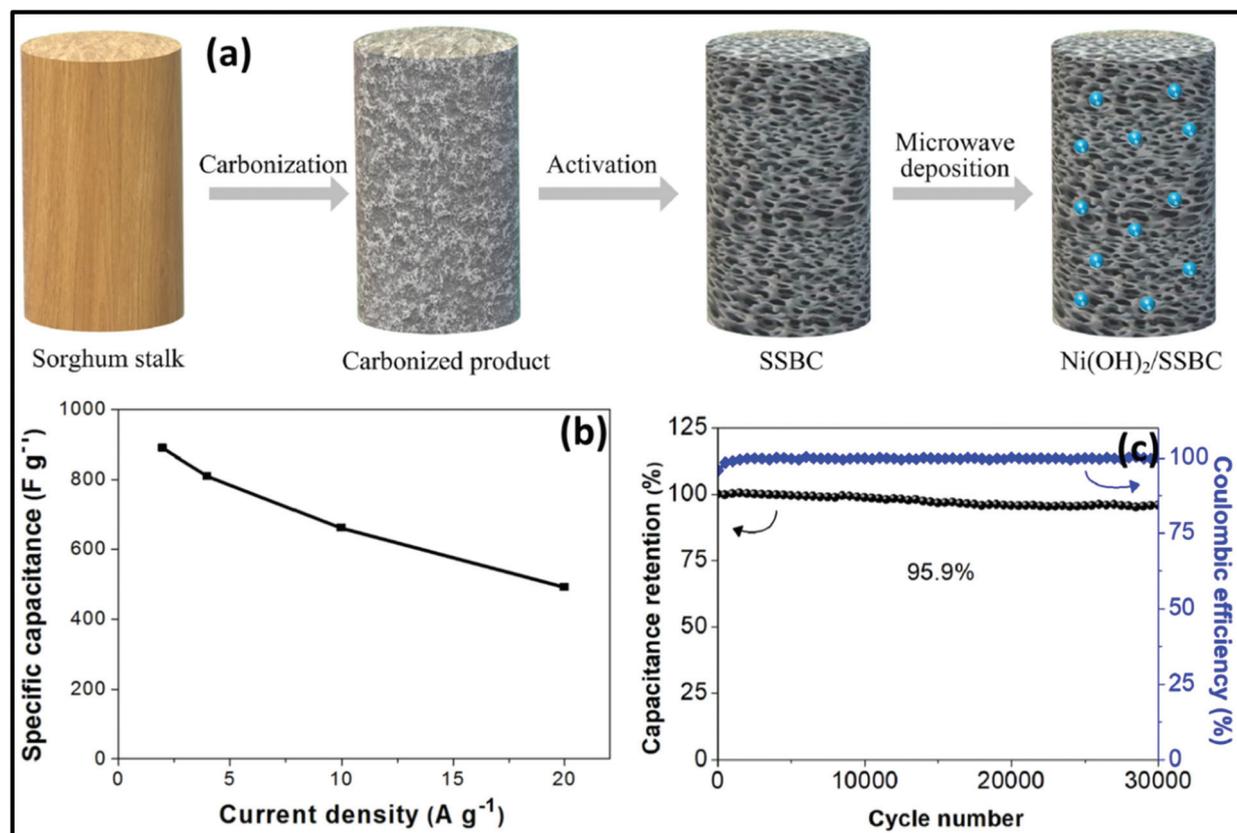
Fig. 18 (a) Synthesis of $Ni(OH)_2$/sorghum stalk biomass carbon, (b) specific capacitance of $Ni(OH)_2$/sorghum stalk biomass carbon composite and (c) cyclic property and columbic efficiency of $Ni(OH)_2$/sorghum stalk biomass carbon composite. Reprinted (adapted) with permission from ref. 267, copyright (2020), Elsevier B.V. All rights reserved.
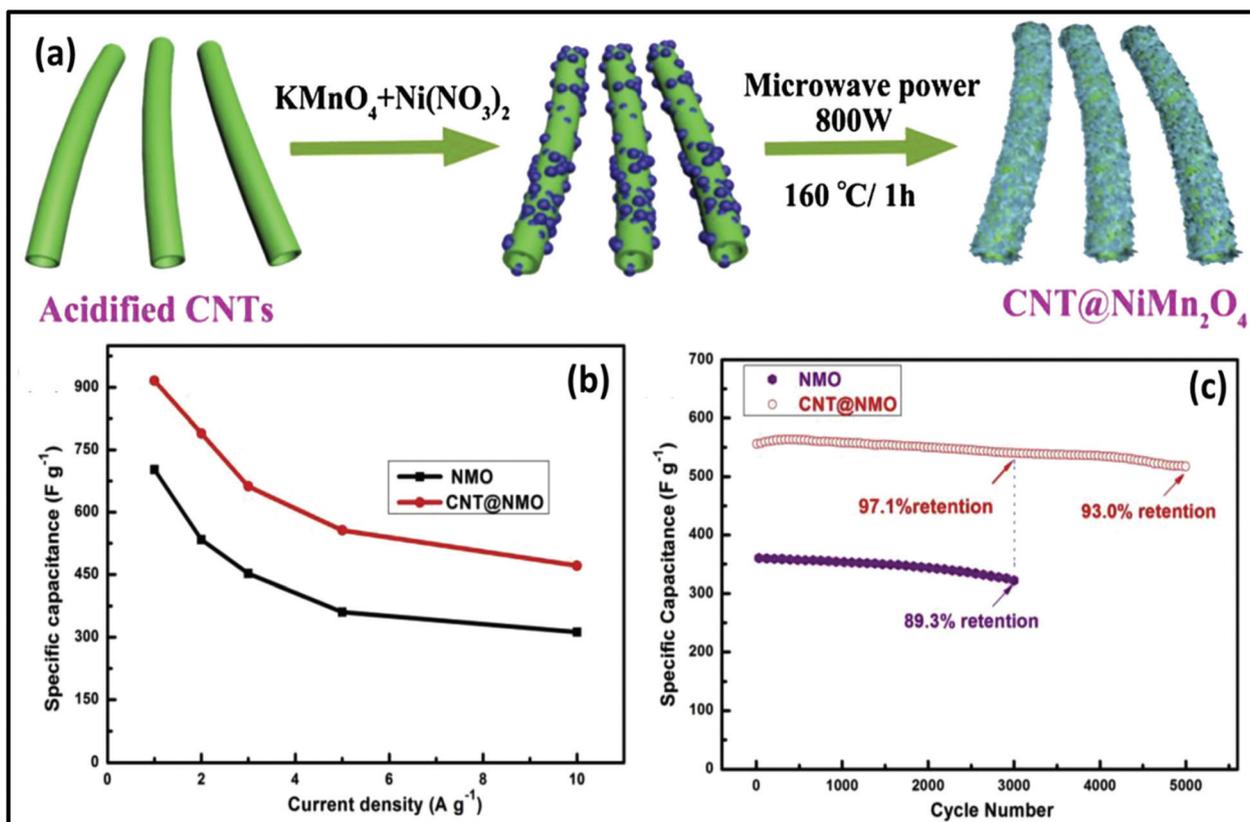
Fig. 19 (a) Schematic representation of the formation of $CNT@NiMn_2O_4$ nanocomposite, (b) specific capacitance of $NiMn_2O_4$ and $CNT@NiMn_2O_4$ nanocomposite at different current densities and (c) cycling stability of $NiMn_2O_4$ and $CNT@NiMn_2O_4$ nanocomposite at 5 A g^{-1}. Reprinted (adapted) with permission from ref. 273, copyright (2020), Elsevier B.V. All rights reserved.
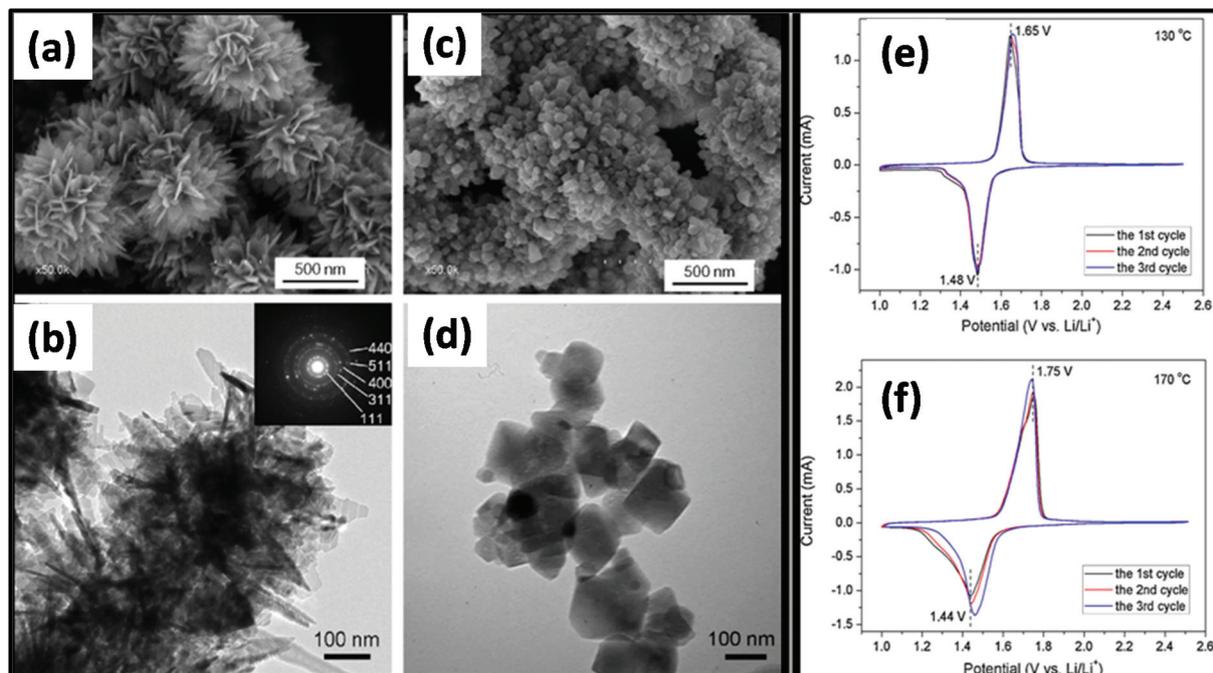
Fig. 20 (a and c) SEM images of $Li_4Ti_5O_{12}$ synthesized at 130 °C and (b and d) TEM images of $Li_4Ti_5O_{12}$ synthesized at 170 °C. (e and f) CV curves of $Li_4Ti_5O_{12}$ prepared at (e) 130 °C and (f) 170 °C in the first three cycles at a scan rate of 0.2 mV s^{-1}.[281] Reprinted (adapted) with permission from ref. 281, copyright (2012), Elsevier B.V. All rights reserved.

assisted synthesis of Fe_3O_4/rGO as a supercapacitor electrode. Crystalline Fe_3O_4 was dispersed on the surface of rGO nanosheets, which avoided the re-aggregation due to the van der Waals interaction between the neighboring rGO sheets. The Fe_3O_4/rGO composite showed a specific capacitance of 972 F g^{-1} at the current density of 1 A g^{-1}, which was higher than that of rGO (251 F g^{-1}) and Fe_3O_4 (183 F g^{-1}).

The MW approach was employed for the synthesis of NiO/NiS@CNT nanocomposites in 60 s for supercapacitors, which exhibited long cycling stability.[270] NiO/NiS@CNT showed a specific capacitance of 809.7 F g^{-1} at 1 A g^{-1} and cycling stability of 100% retention after 20 000 cycles at 5 A g^{-1}. In another study, Zheng et al.[271] reported the synthesis of NiO/Ni_3S_2@graphite nanocomposites via MW as a supercapacitor electrode. Graphite flakes were decorated with NiO/Ni_3S_2, giving the capacitance of 768 F g^{-1} at 1 A g^{-1}. After 1000 cycles, the NiO/Ni_3S_2@graphite electrode showed a specific capacitance of 692 F g^{-1} at 1 A g^{-1} with a capacitance retention of 90%. The NiO/Ni_3S_2@graphite and active carbon electrode-based asymmetric supercapacitor exhibited a specific capacitance of 68.5 F g^{-1} at 1 A g^{-1}, energy density of 28.86 W h kg^{-1} and power density of 0.77 kW kg^{-1} with cycling stability of 80% retention after 2000 cycles. Faid et al.[272] demonstrated the synthesis of ternary mixed $NiCoFeO_4$ nanorods via an MW process as an asymmetric supercapacitor electrode. The synthesized $NiCoFeO_4$ nanorods showed a specific capacitance of 1263 F g^{-1} (at 1 A g^{-1}) and cyclic stability of 97.2% capacitance retention after 2000 cycles. The asymmetric supercapacitor using the $NiCoFeO_4$ nanorods exhibited a power density of 10 kW kg^{-1}, energy density of 9.8 W h kg^{-1}, coulombic efficiency of 95.5%, and capacitance retention of 94% after 4000 cycles. Sun et al.[273] reported the MW-assisted hydrothermal synthesis of a $CNTs@NiMn_2O_4$ core–shell nanocomposite for asymmetric supercapacitors. The schematic representation in Fig. 19a shows the formation of the $CNTs@NiMn_2O_4$ core–shell nanocomposite. The $CNT@NiMn_2O_4$ core–shell nanocomposite exhibited a specific capacitance 915.6 F g^{-1} at a current density of 1 A g^{-1} and cycling stability of 93.0% capacitance retention after 5000 cycles at 5 A g^{-1} (Fig. 19b). The asymmetric supercapacitor device using $CNT@NiMn_2O_4$ as the positive electrode exhibited an energy density of 36.5 W h kg^{-1} at a power density of 800 W kg^{-1} with cycling stability of 82.8% capacitance retention after 10 000 cycles at 5 A g^{-1} (Fig. 19c).

MW-assisted graphene derivatives combined with various types of metal oxides have been used as promising electrode materials for supercapacitors.[274–278] The synthesis of V_2O_5/graphene composites as electrode materials in supercapacitors using the MW method was reported by Fu et al.[279] The V_2O_5/graphene composites were used in symmetrical supercapacitors, demonstrating specific capacitances of 673.2 and 474.6 F g^{-1} at 1 and 10 A g^{-1}, respectively with 96.8% capacitance retention after 10 000 cycles at 1 A g^{-1}. The assembled supercapacitor devices showed an energy density of 46.8 W h kg^{-1} and 32.9 W h kg^{-1} at a power density of 499.4 W kg^{-1} and 4746.0 W kg^{-1}, respectively. Kumar et al.[280] described the synthesis of ZnO nanoparticles anchored on rGO nanosheets via the MW approach for supercapacitor electrodes. The synthesized ZnO@rGO nanocomposite showed a specific capacitance of 102.4 F g^{-1} at 30 mV s^{-1} and cyclic stability of 82.5% for 3000 cycles at 100 mV s^{-1}.

4.5. Batteries

MW-assisted synthesis has also been used for the fabrication of materials for battery applications given that it is simple, cost efficient, not time consuming and nanoparticles with different morphologies can be prepared.[277] MW-assisted hydrothermal synthesis was employed for the synthesis of nanoflower and nanoparticle spinel of $Li_4Ti_5O_{12}$. In this synthesis, LiOH and titanium tetraisopropoxide were used as pre-
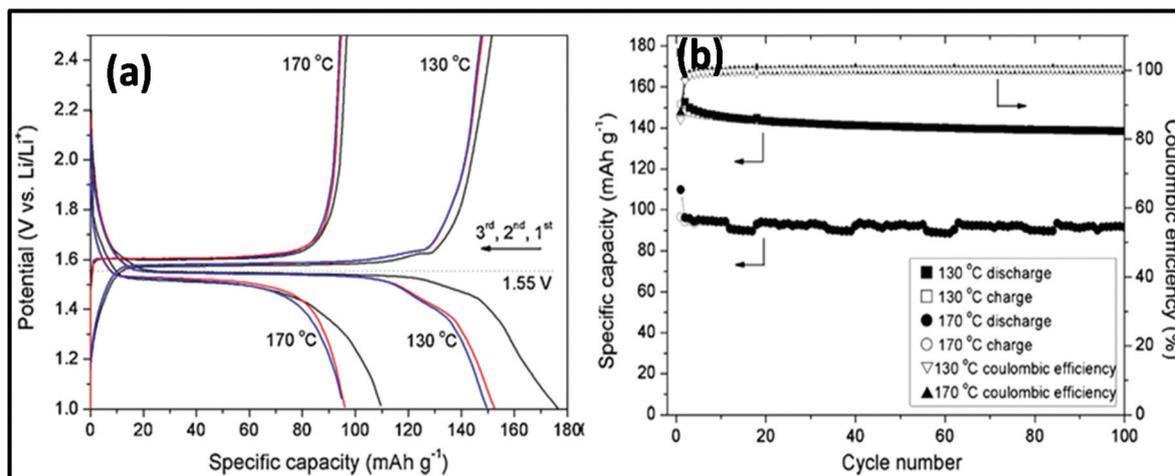
Fig. 21 (a) Galvanostatic charge/discharge curves for $Li_4Ti_5O_{12}$ prepared at 130 °C and 170 °C between 1 and 2.5 V at a current density of 200 mA g^{-1}. (b) Cycling performance of $Li_4Ti_5O_{12}$ prepared at 130 °C and 170 °C measured at a current density of 200 mA g^{-1}.[281] Reprinted (adapted) with permission from ref. 281, copyright (2012), Elsevier B.V. All rights reserved.

cursors with water as the solvent. The synthesis was carried out in an MW-assisted hydrothermal system at 130–170 °C with a holding time of 20 min. Subsequently, the product was calcined at 550 °C for 6 h in air. The morphology of both samples prepared at 130 °C and 170 °C was studied, as shown in Fig. 20a–d. It was found that the sample prepared at 130 °C exhibited a flower-like morphology and that prepared at 170 °C consisted of different-sized nanoparticles. The flower dimensions varied from 500–900 nm and the nanoparticle size varied from tens of nanometers to hundreds of nanometers. The surface area measurements indicated the presence of meso-porous and macroporous nanoparticles, and the calculated surface area of the flower was 48 cm^2 g^{-1} and 12.1 cm^2 g^{-1} for the nanoparticles. Fig. 20e and f show the cyclic CV for the

nanoflowers and nanoparticles of Li$_4$Ti$_5$O$_{12}$, respectively. There were two peaks in both cases, which correspond to the reduction and oxidation of Li. There was a significant voltage difference in both cases, and the anodic and cathodic peaks were not symmetrical. This was because of the slow Li insertion and extraction due to bulk spinel, which was formed due to the agglomeration of the nanoparticles. Also, the overlapping of the peaks for the nanoflower signified good reversibility, whereas in case of spinel, there was no overlapping for each cycle. Fig. 21 shows galvanostatic charge/discharge and cyclic stability study. The first discharge capacity for the nanoflowers and nanoparticles reached 176 mA h g^{-1} and 109.8 mA h g^{-1} with an irreversible cycling capacity of 14% and 12%, respectively.[281] Thus, the MW hydrothermal method is an
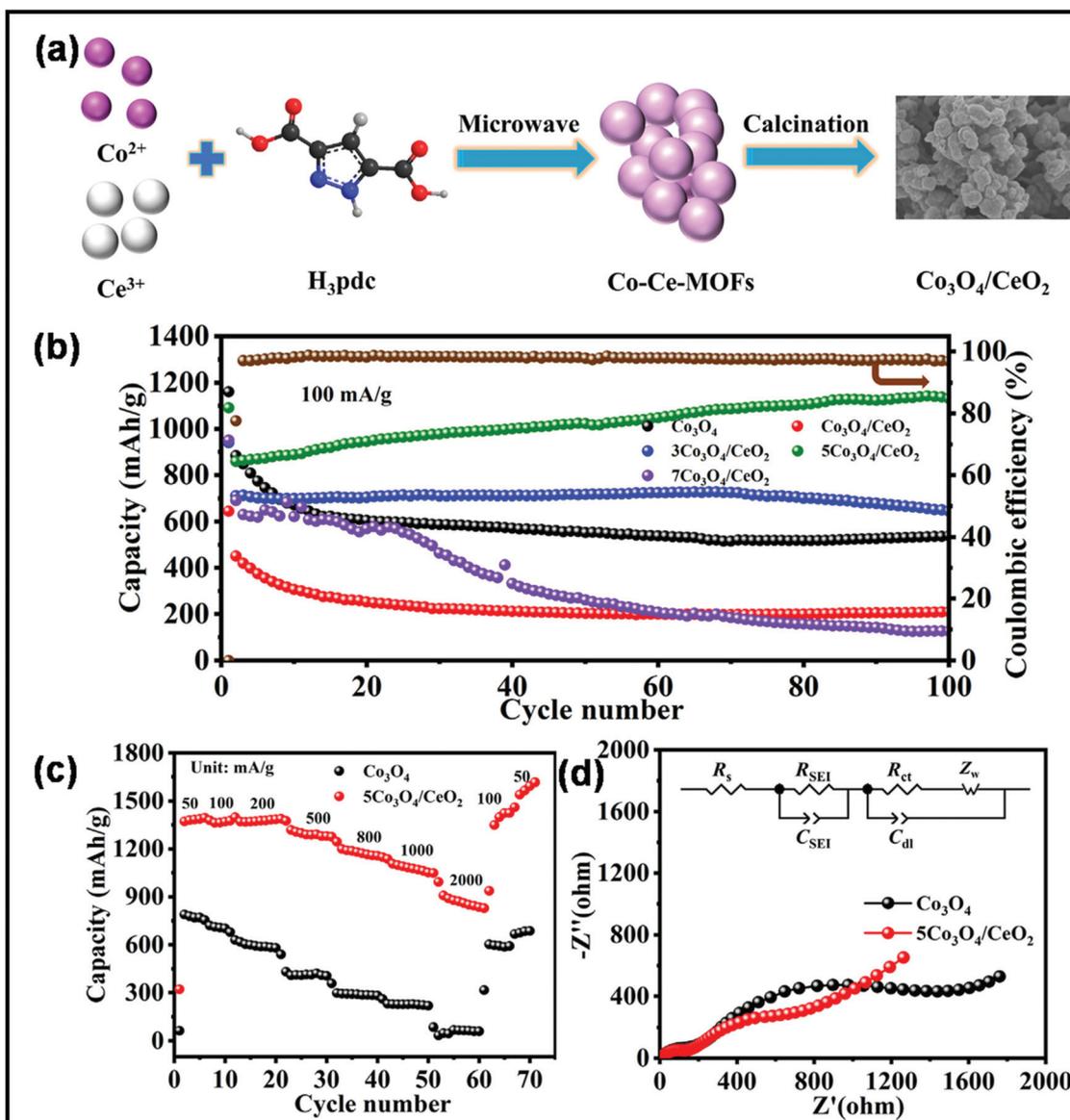
Fig. 22   (a) Schematic illustration of the preparation of Co$_3$O$_4$/CeO$_2$, (b) cycling performance of as-obtained samples at 100 mA g^{-1}, (c) rate performance of Co$_3$O$_4$ and 5Co$_3$O$_4$/CeO$_2$, and (d) Nyquist plots of Co$_3$O$_4$ and 5Co$_3$O$_4$/CeO$_2$ after 100 cycles and the equivalent circuit diagram of the cells.[319] Reprinted (adapted) with permission from ref. 319, copyright (2021), Elsevier B.V. All rights reserved.

efficient method for synthesizing materials for application in batteries. Other reports are also available on the MW synthesis of many other types of nanoparticles. Rai et al.[282] reported the MW synthesis of NiO nanoparticles, which can act as electrode material in Li-ion batteries (LIBs). It was found that these NiO nanoparticles showed a high discharge capacity of 1111.08 mA h g^{-1} and maintained 80% of this capacity after 20 cycles.[282] Also MW-assisted-synthesized Co_3O_4 nanoflakes showed a specific capacity of 883 mA h g^{-1} at a current rate of 0.1C.[283] MW-assisted graphene composites with nanoparticles and metal oxides can also be used as electrode materials for LIBs. Baek et al.[284] synthesized SnO_2 and Fe_3O_4/graphene nanocomposites via a one-pot MW-assisted non-aqueous sol–gel approach for LIBs. There are many more reports showing that MW-assisted methods have the capability to synthesize efficient electrode materials for LIBs.[285,286] MW-assisted-synthesized nanoparticles also showed very good photocatalytic properties. Other authors have also reported similar types of work.[287–289]

In recent years, the MW-assisted approach has significantly improved battery technology.[290–303] Mainly, for the fabrication of secondary battery electrodes, the MW synthetic route has become highly significant.[304–312] Among the various secondary batteries, LIBs are the most popular.[313–318] Accordingly, an anode material based on the Co_3O_4/CeO_2 heterostructure was synthesized in an MW digester at a temperature of 100 °C for 1 h for LIB application.[319] For this MW synthetic process, a Co–Ce metal–organic framework precursor was used. The anode displayed a high capacity of 1131.2 mA h g^{-1} at the current density of 100 mA g^{-1} after 100 charge/discharge

cycles. A schematic of the synthesis process and battery performance of the Co_3O_4/CeO_2 heterostructure are shown in Fig. 22. In a recent report, MW-synthesized high-quality rGO exhibited excellent electrochemical performance for application as both an anode and cathode material for LIBs.[309] For example, as an LIB anode, the rGO electrode exhibited an enhanced capacity of 750 mA h g^{-1}, and as an LIB cathode, it displayed the promising capacity retention of 70%. In another report, an MW-synthesized composite based on $CuC_2O_4 \cdot xH_2O$ and graphene demonstrated excellent electrochemical performances as an anode material for LIB application.[312] With 5.42 wt% graphene, the composite demonstrated the superior discharge/charge capacity of 1043/1013 mA h g^{-1}. Further, an MW-assisted solution combustion process was employed for the synthesis of rGO-wrapped $Li(Ni_{1/3}Co_{1/3}Mn_{1/3})O_2$, which exhibited a discharge capacity of 209.2 mA h g^{-1}.[290] In a recent report, a one-step MW heating process was employed for synthesizing micro/nanoscale $LiFePO_4$/graphene, which exhibited the maximum discharge capacity of 166.3 mA h g^{-1} at the current of 0.1 C.[320] The composite was considered a suitable candidate for next-generation cathode material for LIBs. MW synthesis was further extended to produce an LIB anode material based on Ge/GeO_2 and graphene.[321] The composite exhibited excellent cycling stability.

Recently, Tariq et al. proposed an MW-assisted chemical precipitation technique to synthesize composites of $LiMn_2O_4$ (LMO), CNTs, and graphene nanoplatelets (GNPs).[322] As a cathode material for LIBs, LMO/CNT displayed a discharge capacity of 124 mA h g^{-1}, whereas the LMO/GNP composite exhibited the maximum capacity of 127 mA h g^{-1} at the
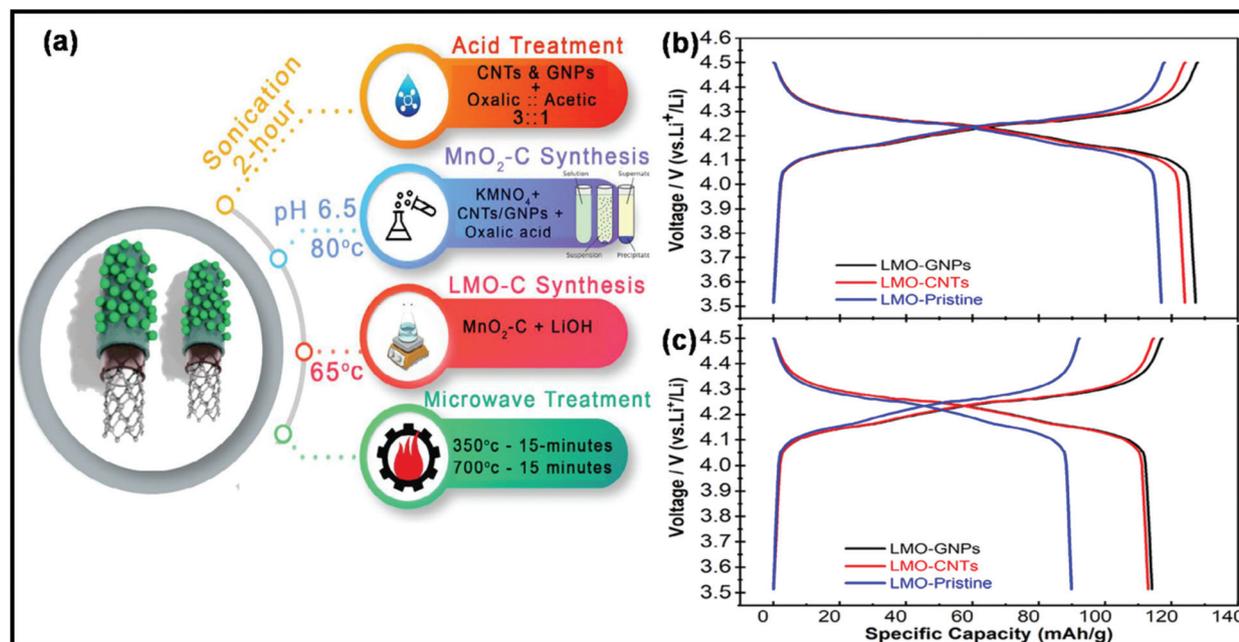
Fig. 23 (a) Schematic of the experimental details for the synthesis of $LiMn_2O_4$/CNT/GNP nanocomposite. (b) Galvanostatic charge/discharge behavior of $LiMn_2O_4$/GNPs, $LiMn_2O_4$-CNTs and pristine $LiMn_2O_4$ at 0.1 C and 25 °C (b) 1st cycle and (c) 50th cycle.[322] Reprinted (adapted) with permission from ref. 322, copyright (2021), Wiley, All rights reserved.

current of 0.1 C. A schematic representation of the synthesis process and the corresponding electrochemical performance of these composites are shown in Fig. 23.

Besides LIBs, the MW approach has also been further extended to Na-ion battery (SIB) applications.[323–328] For example, Mao *et al.*[326] reported an MW-assisted glycerol-mediated hydrothermal process for the synthesis of $Na_3V_2(PO_4)_2F_3$/carbon nanospheres, which exhibited a capacity of 106 mA h g^{-1} at the current of 0.5 C after 100 cycles as a cathode material for SIBs. These recent studies on the MW synthetic approach evidently demonstrate its huge impact and extensive potential in modern science and technology.

5. Conclusions, outlook and future prospective

MW-assisted synthesis has many unique features, which makes it a potentially suitable method for large-scale industrial production. MW heating is fast and uniform due to volumetric and dielectric heating, resulting in selective heating processes. In the case of conventional heating, heating is due to conduction and convection and heat transfers from one molecule to another. This phenomenon restricts uniform temperature and is slow. Conversely, MW heating is dielectric heating due to the ions and dipoles in materials, which readily interact with radiation. The delay in the flipping of dipoles and ions while trying to flip their direction with the phase of electromagnetic radiation is called the relaxation time. This relaxation results in the loss of energy, which is liberated in the form of heat. The nature of these interactions is different for different materials. In carbon materials, MW heating involves different mechanisms besides ionic and dielectric heating and involves free electrons. The exposure of MWI to organic reactions is less compared to inorganic materials because of the non-polar nature of organic solvents. MW is used in organic reactions nowadays because the dielectric property varies with temperature and water/other liquids can be used as a solvent at high temperatures. Most of the organic reactions are carried out by MW heating using water as the solvent. Also, many reactions show that the reaction rates and product yield increase in the presence of MWI. Thus, many metal oxides, metal hydroxides, and organic materials have been synthesized by employing MW heating. In the case of carbon materials, generally, heterogeneous nucleation occurs, given that in these composites, the carbon materials act as the substrate during the synthesis. Various shapes, sizes, and morphologies of materials can be controlled easily with MWI. MWI-assisted hydrothermal and solvothermal processes for the synthesis of nanomaterials are less time consuming, which in most cases takes very long for completion. The MW-assisted-synthesized products can be further employed for many energy storage and conversion applications such as supercapacitors, batteries, and photovoltaics. Thus, MWI makes the synthesis of materials much more feasible, cost

effective, and selective for commercial applications and large-scale industrial production.

Herein, we delivered a brief, selective, and systematic literature review on the MW-assisted synthesis and energy-related application of carbon nanomaterials and metal oxides/hydroxides. Although ample work has already been done in this hot field, the MW-assisted synthesis process has some drawbacks. Mainly, in terms of commercial aspects, the MW route is still not popular. Among the various energy storage devices, supercapacitors and secondary batteries are considered as the best solutions for the ever-growing demand of future electronics. Accordingly, due to its shorter reaction time, the MW synthetic route has huge potential for the construction of these devices. Besides energy storage devices, the MW approach has been extended to other applications including EMI shielding, wastewater treatment, bio-medical application, fuel cells, and solar cells. Therefore, future advancement in MW chemistry will be highly beneficial for mankind. The future prospective of MW technology is discussed in the next section.

As discussed in the previous section, the MW synthesis approach has several advantages and can be considered as a star technology in the future. However, to make this approach commercially viable, researchers need to focus on few features. The future research on MW technology can be directed towards the follow points

1. The basic mechanism of MW heating has not been clearly understood to date. Thus, more fundamental research on this topic is highly required.

2. For large-scale production, MW technology has several drawbacks. The production of MW reactors for large batches with high yield and excellent repeatability is extremely advantageous.

3. The heating is very fast and the heat transfer to surrounding media (gas or liquid) is relatively slow, and very high temperatures not obtainable under the common thermal equilibrium conditions can be reached. To enhance the uniformity, a proper absorber needs to be chosen and the penetration depth and frequency of the electromagnetic waves controlled. Homogeneous heating can improve the quality of the product.

4. For battery applications, the initial decay in capacity after the 1st cycle is associated with the formation of a solid electrolyte interface (SEI). Future research on carbon nanomaterials should be focused on reducing the formation of the SEI.

5. For supercapacitor applications, the smart combination of EDLC-type (such as carbon nanomaterials) and pseudocapacitive (metal oxide or conducting polymers) materials is highly desirable. MW technology should be broadly extended to combine carbon materials with other suitable materials. It is important to note that recently, the MW approach has been extended towards the development of these smart combinations.

6. Detailed theoretical investigation on isotropic and anisotropic MW heating can open a new door for future research in this field.

Lastly, MW technology is growing exponentially daily. However, still this technology has a way to go for its commercialization.

Conflicts of interest

There are no conflicts to declare.

Acknowledgements

Notes and references

1 M. A. Bagherian and K. Mehranzamir, *Energy Convers. Manage.*, 2020, **224**, 113454.

2 L. Li, J. Lin, N. Wu, S. Xie, C. Meng, Y. Zheng, X. Wang and Y. Zhao, *Energy Built Environ.*, 2020, DOI: 10.1016/j. enbenv.2020.12.002.

3 M. S. Nazir, M. Bilal, H. M. Sohail, B. Liu, W. Chen and H. M. N. Iqbal, *Int. J. Hydrogen Energy*, 2020, **45**, 22113–22124.

4 K. Ravindra, M. Kaur-Sidhu and S. Mor, *Sci. Total Environ.*, 2021, 145657, DOI: 10.1016/j. scitotenv.2021.145657.

5 M. M. Vanegas Cantarero, *Energy Res. Soc. Sci.*, 2020, **70**, 101716.

6 G. Q. Chen, J. S. Li, B. Chen, C. Wen, Q. Yang, A. Alsaedi and T. Hayat, *Renewable Sustainable Energy Rev.*, 2016, **65**, 345–355.

7 M. E. Munawer, *J. Sustainable Min.*, 2018, **17**, 87–96.

8 J. Pei, Y. Wen, Y. Li, X. Shi, J. Zhang, R. Li and Q. Du, *Constr. Build. Mater.*, 2014, **72**, 41–47.

9 K. Yin, A. Ahamed and G. Lisak, *Waste Manage.*, 2018, **78**, 401–416.

10 B. Esser, F. Dolhem, M. Becuwe, P. Poizot, A. Vlad and D. Brandell, *J. Power Sources*, 2021, **482**, 228814.

11 M. Fu, Z. Zhang, Z. Zhu, Q. Zhuang, W. Chen, H. Yu and Q. Liu, *J. Colloid Interface Sci.*, 2021, **588**, 795–803.

12 B. Gang, F. Zhang, X. Li, B. Zhai, X. Wang and Y. Song, *J. Energy Storage*, 2021, **33**, 102132.

13 Y. Ge, Z. Liu, Y. Wu and R. Holze, *Electrochim. Acta*, 2021, **366**, 137390.

14 O. Gorduk, M. Gencten, S. Gorduk, M. Sahin and Y. Sahin, *J. Energy Storage*, 2021, **33**, 102049.

15 Y. He, X. Yuan, G. Zhang, H. Wang, T. Zhang, W. Xie and L. Li, *Sci. Total Environ.*, 2020, **766**, 142382.

16 Y. Pan, E. Yu, D. Wang and H. Deng, *J. Alloys Compd.*, 2021, **858**, 157662.

17 L. Zhang, W. Wang, X. Ma, S. Lu and Y. Xiang, *Nano Today*, 2021, **37**, 101074.

18 M. Zhang, W. Zhou and W. Huang, *J. Energy Chem.*, 2021, **57**, 291–303.

19 L. Zhao, Z. Sun, H. Wan, H. Liu, D. Wu, X. Wang and X. Cui, *Electrochim. Acta*, 2020, **354**, 136718.

20 L. Zheng, H. Yang, Y. Bai and C. Wu, *J. Energy Chem.*, 2021, **60**, 229–232.

21 R. Kumar, E. Joanni, R. Savu, M. S. Pereira, R. K. Singh, C. J. L. Constantino, L. T. Kubota, A. Matsuda and S. A. Moshkalev, *Energy*, 2019, **179**, 676–684.

22 R. Kumar, S. Sahoo, E. Joanni, R. K. Singh, W. K. Tan, K. K. Kar and A. Matsuda, *Prog. Energy Combust. Sci.*, 2019, **75**, 100786.

23 R. Kumar, R. K. Singh, D. P. Singh, E. Joanni, R. M. Yadav and S. A. Moshkalev, *Coord. Chem. Rev.*, 2017, **342**, 34–79.

24 R. Kumar, E. Joanni, R. K. Singh, D. P. Singh and S. A. Moshkalev, *Prog. Energy Combust. Sci.*, 2018, **67**, 115–157.

25 R. Kumar, S. Sahoo, E. Joanni, R. K. Singh, R. M. Yadav, R. K. Verma, D. P. Singh, W. K. Tan, A. Pérez del Pino, S. A. Moshkalev and A. Matsuda, *Nano Res.*, 2019, **12**, 2655–2694.

26 R. Kumar, H.-J. Kim, S. Park, A. Srivastava and I.-K. Oh, *Carbon*, 2014, **79**, 192–202.

27 V. S. Avvaru, I. J. Fernandez, W. Feng, S. J. Hinder, M. C. Rodríguez and V. Etacheri, *Carbon*, 2021, **171**, 869–881.

28 M. Hu, H. Zhang and R. Lv, *Prog. Nat. Sci.: Mater. Int.*, 2020, **30**, 20–27.

29 J.-M. Lim, S. Kim, N. S. Luu, J. R. Downing, M. T. Z. Tan, K.-Y. Park, J. C. Hechter, V. P. Dravid, K. He and M. C. Hersam, *Matter*, 2020, **3**, 522–533.

30 Q. Wang and W. A. Daoud, *J. Power Sources Adv.*, 2020, **4**, 100018.

31 J. Wen, D. Zhao and C. Zhang, *Renewable Energy*, 2020, **162**, 1629–1648.

32 X. Xu, J. Yang, X. Zhou, S. Jiang, W. Chen and Z. Liu, *Chem. Eng. J.*, 2020, **397**, 125525.

33 Z. Yang, J. Tian, Z. Ye, Y. Jin, C. Cui, Q. Xie, J. Wang, G. Zhang, Z. Dong, Y. Miao, X. Yu, W. Qian and F. Wei, *Energy Storage Mater.*, 2020, **33**, 18–25.

34 S. Zhang, B. S. Huang, C. Shi, Q. Xu and Y. Zhu, *Colloids Surf., A*, 2020, **605**, 125243.

35 R. Kumar, E. Joanni, R. K. Singh, E. T. S. G. da Silva, R. Savu, L. T. Kubota and S. A. Moshkalev, *J. Colloid Interface Sci.*, 2017, **507**, 271–278.

36 J. Bi, H. Wu, L. Wang, X. Pang, Y. Li, Q. Meng and L. Wang, *Electrochim. Acta*, 2021, **367**, 137409.

37 Z. Fan, J. Chen, B. Zhang, F. Sun, B. Liu and Y. Kuang, *Mater. Res. Bull.*, 2008, **43**, 2085–2091.

38 Y. Huang, H. Wang, Y. Jiang and X. Jiang, *Mater. Lett.*, 2020, **276**, 128261.

39 S. J. Keszei, P. Pekker, C. Fehér, S. Balogh, M. Jakab, L. Nagy and R. Skoda-Földes, *Microporous Mesoporous Mater.*, 2020, **308**, 110380.

40 R. Kumar, R. Savu, E. Joanni, A. R. Vaz, M. A. Canesqui, R. K. Singh, R. A. Timm, L. T. Kubota and S. A. Moshkalev, *RSC Adv.*, 2016, **6**, 84769–84776.

41 J. Lin, L. Sun, Z. Cao, D. Yin, F. Liang, Y. Wu and L. Wang, *Electrochim. Acta*, 2016, **222**, 1716–1723.

42 Z. Liu, C. Pan, W. Li, S. Wei, M. Zhang and S. Chen, *Electrochim. Acta*, 2020, **338**, 135897.

43 Z. Liu, D. Tian, F. Shen, P. C. Nnanna, J. Hu, Y. Zeng, G. Yang, J. He and S. Deng, *J. Power Sources*, 2020, **458**, 228057.

44 G. Qu, Y. Zhou, J. Zhang, L. Xiong, Q. Yue and Y. Kang, *iScience*, 2020, **23**, 101396.

45 R. Kumar, R. K. Singh and D. P. Singh, *Renewable Sustainable Energy Rev.*, 2016, **58**, 976–1006.

46 N. Wang, Y. Wu, G. Han, H. Song, W. Hou and H. Wang, *Diamond Relat. Mater.*, 2020, **105**, 107766.

47 H. Wu, L. Lu, Y. Zhang, Z. Sun and L. Qian, *Colloids Surf., A*, 2016, **502**, 26–33.

48 P. Zhang, Y. Yang, Z. Ma, Y. Wang, Y. Pan and C. Lu, *Mater. Lett.*, 2016, **164**, 421–424.

49 R. Kumar, R. K. Singh, P. K. Dubey, D. P. Singh, R. M. Yadav and R. S. Tiwari, *Adv. Mater. Interfaces*, 2015, **2**, 1500191.

50 Z. Zheng, Y. Du, Q. Feng, Z. Wang and C. Wang, *J. Mol. Catal. A: Chem.*, 2012, **353–354**, 80–86.

51 Q. Zhou, M. Bao and X. Ni, *Surf. Coat. Technol.*, 2021, **406**, 126660.

52 S. M. Youssry, I. S. El-Hallag, R. Kumar, G. Kawamura, A. Matsuda and M. N. El-Nahass, *J. Electroanal. Chem.*, 2020, **857**, 113728.

53 C. Antonio and R. T. Deam, *J. Mater. Process. Technol.*, 2005, **169**, 234–241.

54 S. S. R. Geedipalli, V. Rakesh and A. K. Datta, *J. Food Eng.*, 2007, **82**, 359–368.

55 J. He, Y. Yang, H. Zhu, K. Li, W. Yao and K. Huang, *Appl. Therm. Eng.*, 2020, **178**, 115594.

56 D. Jain, J. Tang, F. Liu, Z. Tang and P. D. Pedrow, *Innovative Food Sci. Emerging Technol.*, 2018, **48**, 274–286.

57 S. Taghian Dinani, M. Hasić, M. Auer and U. Kulozik, *Food Bioprod. Process.*, 2020, **124**, 121–130.

58 H. Zhu, J. He, T. Hong, Q. Yang, Y. Wu, Y. Yang and K. Huang, *Appl. Therm. Eng.*, 2018, **141**, 648–658.

59 F. Gulisano and J. Gallego, *Constr. Build. Mater.*, 2021, **278**, 121993.

60 L. Hou, Y. Zhang, L. Chen and X. Wang, *LWT*, 2021, **139**, 110614.

61 P. Song, Y. Lei, X. Hu, C. Wang, J. Wang and Y. Tang, *J. Colloid Interface Sci.*, 2020, **574**, 421–429.

62 T. A. Thu Dao, H. K. Webb and F. Malherbe, *Food Hydrocolloids*, 2021, **113**, 106475.

63 D. Wu, W. Sun, S. Liu and C. Qu, *Constr. Build. Mater.*, 2021, **266**, 121180.

64 Q. Ye, Z. Peng, G. Li, Y. Liu, M. Liu, L. Ye, L. Wang, M. Rao and T. Jiang, *J. Cleaner Prod.*, 2021, **286**, 124919.

65 R. K. Singh, R. Kumar, D. P. Singh, R. Savu and S. A. Moshkalev, *Mater. Today Chem.*, 2019, **12**, 282–314.

66 T. Ichikawa, T. Matsuo, T. Tachikawa, T. Yamada, T. Yoshimura, M. Yoshimura, Y. Takagi, Y. Sawama, J.-i. Sugiyama, Y. Monguchi and H. Sajiki, *ACS Sustainable Chem. Eng.*, 2019, **7**, 3052–3061.

67 A.-M. Galan, I. Calinescu, A. Trifan, C. Winkworth-Smith, M. Calvo-Carrascal, C. Dodds and E. Binner, *Chem. Eng. Process.*, 2017, **116**, 29–39.

68 J. Y. Xing, X. L. Song, B. Bai, S. K. Lu and H. P. Liu, *Appl. Mech. Mater.*, 2014, **448–453**, 3005–3008.

69 T. Sumi and S. Horikoshi, *Radiat. Phys. Chem.*, 2015, **114**, 31–37.

70 M. T. Bevacqua, T. Isernia, F. G. Praticò and S. Zumbo, *Autom. Constr.*, 2021, **121**, 103426.

71 J. Fukushima and H. Takizawa, *Mater. Chem. Phys.*, 2016, **172**, 47–53.

72 S. Horikoshi, M. Kamata, T. Sumi and N. Serpone, *Int. J. Hydrogen Energy*, 2016, **41**, 12029–12037.

73 C. S. Lee, E. Binner, C. Winkworth-Smith, R. John, R. Gomes and J. Robinson, *Chem. Eng. Sci.*, 2016, **149**, 97–103.

74 D. Nagao, J. Fukushima, Y. Hayashi and H. Takizawa, *Ceram. Int.*, 2015, **41**, 14021–14028.

75 K. Wang, G. Dimitrakis and D. J. Irvine, *Chem. Eng. Process.*, 2017, **122**, 389–396.

76 M. B. Gawande, S. N. Shelke, R. Zboril and R. S. Varma, *Acc. Chem. Res.*, 2014, **47**, 1338–1348.

77 J. Menéndez, A. Arenillas, B. Fidalgo, Y. Fernández, L. Zubizarreta, E. G. Calvo and J. M. Bermúdez, *Fuel Process. Technol.*, 2010, **91**, 1–8.

78 R. Kumar, R. Savu, R. K. Singh, E. Joanni, D. P. Singh, V. S. Tiwari, A. R. Vaz, E. T. S. G. da Silva, J. R. Maluta, L. T. Kubota and S. A. Moshkalev, *Carbon*, 2017, **117**, 137–146.

79 R. Kumar, E. T. S. G. da Silva, R. K. Singh, R. Savu, A. V. Alaferdov, L. C. Fonseca, L. C. Carossi, A. Singh, S. Khandka, K. K. Kar, O. L. Alves, L. T. Kubota and S. A. Moshkalev, *J. Colloid Interface Sci.*, 2018, **515**, 160–171.

80 L. V. Kumar, S. Addo Ntim, O. Sae-Khow, C. Janardhana, V. Lakshminarayanan and S. Mitra, *Electrochim. Acta*, 2012, **83**, 40–46.

81 Z. Q. Tian, X. L. Wang, H. M. Zhang, B. L. Yi and S. P. Jiang, *Electrochem. Commun.*, 2006, **8**, 1158–1162.

82 A. Bharti, G. Cheruvally and S. Muliankeezhu, *Int. J. Hydrogen Energy*, 2017, **42**, 11622–11631.

83 X. Hu, P. Song, X. Yang, C. Wang, J. Wang, Y. Tang, J. Zhang and Z. Mao, *J. Taiwan Inst. Chem. Eng.*, 2020, **115**, 272–278.

84 L. L. Sikeyi, T. D. Ntuli, T. H. Mongwe, N. W. Maxakato, E. Carleschi, B. P. Doyle, N. J. Coville and M. S. Maubane-Nkadimeng, *Int. J. Hydrogen Energy*, 2021, **46**, 10862–10875.

85 S. Mahalingam, S. Ayyaru and Y.-H. Ahn, *Chemosphere*, 2021, **278**, 130426.

86 X. Feng, H. Dai, J. Zhu, L. Ma, Y. Yu, H. Zhu, H. Wang, Y. Sun, H. Tan and Y. Zhang, *Int. J. Biol. Macromol.*, 2021, **171**, 1–9.

87 X. Gui, Y. Chen, Z. Zhang, L. Lei, F. Zhu, W. Yang, Y. Guo and M. Chu, *Biomaterials*, 2020, **248**, 120009.

88 H. Jia, T. Wang, W. Chen, S. Ding, T. Luo and Q. Sun, *Cold Reg. Sci. Technol.*, 2021, **184**, 103248.

89 N. Lee, J. H. Bang, H. W. Kim and H. Jeon, *Ceram. Int.*, 2020, **47**(8), 10628–10634.

90 M. Ma, Y. Zhang, X. Chen, H. Li, Z. Sui and H. Corke, *J. Cereal Sci.*, 2020, **95**, 103072.

91 D. Souri, N. Salimi and M. Ghabooli, *Inorg. Chem. Commun.*, 2021, **123**, 108345.

92 Y. Wang, T. Chen, C. Huang, Y. Wang, J. Wu and B. Sun, *J. Electroanal. Chem.*, 2020, **867**, 114181.

93 Y. Yin, C. Ma, W. Li, S. Luo, Y. Liu, X. Wu, Z. Wu and S. Liu, *Ind. Crops Prod.*, 2021, **160**, 113091.

94 X. Zhang, Z. Chen, J. Zhang, X. Ye and S. Cui, *Chem. Phys. Lett.*, 2021, **762**, 138127.

95 A. Metaxas, *Power Eng. J.*, 1991, **5**, 237–247.

96 F. Langa, P. de la Cruz, A. de la Hoz, A. Díaz-Ortiz and E. Díez-Barra, *Contemp. Org. Synth.*, 1997, **4**, 373–386.

97 E. T. Thostenson and T. W. Chou, *Composites, Part A*, 1999, **30**, 1055–1071.

98 S. Chandrasekaran, S. Ramanathan and T. Basak, *Food Res. Int.*, 2013, **52**, 243–261.

99 Y. Zhang, W. Zhao, B. Li and G. Xie, *J. Energy Resour. Technol.*, 2018, **140**(4), 040802.

100 J. E. Omoriyekomwan, A. Tahmasebi, J. Dou, R. Wang and J. Yu, *Fuel Process. Technol.*, 2021, **214**, 106686.

101 P. Chen, Q. Xie, M. Addy, W. Zhou, Y. Liu, Y. Wang, Y. Cheng, K. Li and R. Ruan, *Bioresour. Technol.*, 2016, **215**, 163–172.

102 J. E. Omoriyekomwan, A. Tahmasebi, J. Zhang and J. Yu, *Energy Convers. Manage.*, 2019, **192**, 88–99.

103 J. Sun, W. Wang and Q. Yue, *Materials*, 2016, **9**, 231.

104 D. Stuerga, *Microwaves Org. Synth.*, 2006, **2**, 1–59.

105 H. Fröhlich, 1949, *Theory of dielectrics; dielectric constant and dielectric loss*, Oxford, Clarendon Press.

106 B. Wathey, J. Tierney, P. Lidström and J. Westman, *Drug Discovery Today*, 2002, **7**, 373–380.

107 Y. Ma, E. Vileno, S. L. Suib and P. K. Dutta, *Chem. Mater.*, 1997, **9**, 3023–3031.

108 M. Oghbaei and O. Mirzaee, *J. Alloys Compd.*, 2010, **494**, 175–189.

109 D. E. Clark, D. C. Folz and J. K. West, *Mater. Sci. Eng., A*, 2000, **287**, 153–158.

110 K. D. Raner, C. R. Strauss, F. Vyskoc and L. Mokbel, *J. Org. Chem.*, 1993, **58**, 950–953.

111 J. Berlan, P. Giboreau, S. Lefeuvre and C. Marchand, *Tetrahedron Lett.*, 1991, **32**, 2363–2366.

112 W. C. Sun, P. M. Guy, J. H. Jahngen, E. F. Rossomando and E. G. Jahngen, *J. Org. Chem.*, 1988, **53**, 4414–4416.

113 D. Stuerga, K. Gonon and M. Lallemant, *Tetrahedron*, 1993, **49**, 6229–6234.

114 T. Kim, J. Lee and K.-H. Lee, *Carbon Lett.*, 2014, **15**, 15–24.

115 N. Devi, R. Kumar and R. K. Singh, in *Graphene Functionalization Strategies: From Synthesis to Applications*, ed. A. Khan, M. Jawaid, B. Neppolian and A. M. Asiri, Springer Singapore, Singapore, 2019, pp. 279–311, DOI: 10.1007/978-981-32-9057-0_12.

116 J.-K. Yang and Y.-M. Wu, *Fuel*, 1987, **66**, 1745–1747.

117 S. Marland, A. Merchant and N. Rowson, *Fuel*, 2001, **80**, 1839–1849.

118 Z. Fang, C. Li, J. Sun, H. Zhang and J. Zhang, *Carbon*, 2007, **45**, 2873–2879.

119 S. Challa, W. Little and C. Cha, *J. Microwave Power Electromagn. Energy*, 1994, **29**, 131–137.

120 K. Wu, T. Ting, G. Wang, C. Yang and C. Tsai, *Synth. Met.*, 2008, **158**, 688–694.

121 J. Ma, M. Fang, P. Li, B. Zhu, X. Lu and N. Lau, *Appl. Catal., A*, 1997, **159**, 211–228.

122 J. Atwater and R. Wheeler, *J. Mater. Sci.*, 2004, **39**, 151–157.

123 J. E. Atwater and R. R. Wheeler Jr., *Carbon*, 2003, **41**, 1801–1807.

124 J. Atwater and R. Wheeler Jr., *Appl. Phys. A*, 2004, **79**, 125–129.

125 E. A. Dawson, G. Parkes, P. A. Barnes, G. Bond and R. Mao, *Carbon*, 2008, **46**, 220–228.

126 H. Lin, H. Zhu, H. Guo and L. Yu, *Mater. Res. Bull.*, 2008, **43**, 2697–2702.

127 L. Zhang and H. Zhu, *Mater. Lett.*, 2009, **63**, 272–274.

128 Y. Yao, A. Jänis and U. Klement, *J. Mater. Sci.*, 2008, **43**, 1094–1101.

129 J. Menéndez, A. Domínguez, Y. Fernández and J. Pis, *Energy Fuels*, 2007, **21**, 373–378.

130 K. Majdzadeh-Ardakani and M. M. B. Holl, *Prog. Mater. Sci.*, 2017, **87**, 221–245.

131 P. Monsef-Mirzai, M. Ravindran, W. R. McWhinnie and P. Burchill, *Fuel*, 1995, **74**, 20–27.

132 A. Mokhlisse, M. B. Chanâa and A. Outzourhit, *Fuel*, 2000, **79**, 733–742.

133 A. Zlotorzynski, *Crit. Rev. Anal. Chem.*, 1995, **25**, 43–76.

134 K. E. Haque, *Int. J. Miner. Process.*, 1999, **57**, 1–24.

135 D. A. Jones, T. Lelyveld, S. Mavrofidis, S. Kingman and N. Miles, *Resour., Conserv. Recycl.*, 2002, **34**, 75–90.

136 Y. Fernández, B. Fidalgo, A. Domínguez, A. Arenillas and J. Á. Menéndez, *Carbon*, 2007, **45**(8), 1706–1709.

137 B. Fidalgo, Y. Fernández, L. Zubizarreta, A. Arenillas, A. Domínguez, J. Pis and J. Menéndez, *Appl. Surf. Sci.*, 2008, **254**, 3553–3557.

138 F.-H. Ko, C.-Y. Lee, C.-J. Ko and T.-C. Chu, *Carbon*, 2005, **43**, 727–733.

139 Y. Wang, Z. Iqbal and S. Mitra, *Carbon*, 2005, **43**, 1015–1020.

140 T. Wei, Z. Fan, G. Luo, C. Zheng and D. Xie, *Carbon*, 2009, **47**, 337–339.

141 G. A. Tompsett, W. C. Conner and K. S. Yngvesson, *ChemPhysChem*, 2006, **7**, 296–319.

142 H. I. Lee, J. H. Kim, S. H. Joo, H. Chang, D. Seung, O.-S. Joo, D. J. Suh, W.-S. Ahn, C. Pak and J. M. Kim, *Letters to the Editor*, 2007, **45**, 2843–2854.

143 L. M. Norman and C. Cha, *Chem. Eng. Commun.*, 1995, **140**, 87–110.

144 P. Monsef-Mirzai, M. Ravindran, W. R. McWhinnie and P. Burchill, *Fuel*, 1992, **71**, 716–717.

145 M. B. Chanaa, M. Lallemant and A. Mokhlisse, *Fuel*, 1994, **73**, 1643–1649.

146 J. Menéndez, M. Inguanzo and J. Pis, *Water Res.*, 2002, **36**, 3261–3264.

147 Y. Li, M. A. Malik and P. O'Brien, *J. Am. Chem. Soc.*, 2005, **127**, 16020–16021.

148 J. A. Dahl, B. L. Maddux and J. E. Hutchison, *Chem. Rev.*, 2007, **107**, 2228–2269.

149 L. Zhang, X. Hai, C. Xia, X.-W. Chen and J.-H. Wang, *Sens. Actuators, B*, 2017, **248**, 374–384.

150 D. L. Boxall and C. Lukehart, *Chem. Mater.*, 2001, **13**, 806–810.

151 J. Liang, Z. Deng, X. Jiang, F. Li and Y. Li, *Inorg. Chem.*, 2002, **41**, 3602–3604.

152 R. Harpeness and A. Gedanken, *Langmuir*, 2004, **20**, 3431–3434.

153 J. A. Gerbec, D. Magana, A. Washington and G. F. Strouse, *J. Am. Chem. Soc.*, 2005, **127**, 15791–15800.

154 A. B. Panda, G. Glaspell and M. S. El-Shall, *J. Am. Chem. Soc.*, 2006, **128**, 2790–2791.

155 S. Kundu, L. Peng and H. Liang, *Inorg. Chem.*, 2008, **47**, 6344–6352.

156 H.-Q. Wang and T. Nann, *ACS Nano*, 2009, **3**, 3804–3808.

157 A. F. Zedan, S. Sappal, S. Moussa and M. S. El-Shall, *J. Phys. Chem. C*, 2010, **114**, 19920–19927.

158 V. K. LaMer and R. H. Dinegar, *J. Am. Chem. Soc.*, 1950, **72**, 4847–4854.

159 K. F. Kelton, in *Solid state physics*, Elsevier, 1991, vol. 45, pp. 75–177.

160 B. Peters, *J. Chem. Phys.*, 2011, **135**, 044107.

161 N. P. Herring, A. B. Panda, K. AbouZeid, S. H. Almahoudi, C. R. Olson, A. Patel and M. El-Shall, in *Metal Oxide Nanomaterials for Chemical Sensors*, Springer, 2013, pp. 245–284.

162 I. Bilecka, P. Elser and M. Niederberger, *ACS Nano*, 2009, **3**, 467–477.

163 M. Yada, H. Kitamura, A. Ichinose, M. Machida and T. Kijima, *Angew. Chem., Int. Ed.*, 1999, **38**, 3506–3510.

164 R. Si, Y. W. Zhang, L. P. You and C. H. Yan, *Angew. Chem., Int. Ed.*, 2005, **44**, 3256–3260.

165 A. B. Panda, G. Glaspell and M. S. El-Shall, *J. Phys. Chem. C*, 2007, **111**, 1861–1864.

166 H. Huang, S. Sithambaram, C. H. Chen, C. K. Kithongo, L. Xu, A. Iyer, H. F. Garces and S. L. Suib, *Chem. Mater.*, 2010, **22**, 3664–3669.

167 Z. Chen, J. Li, Y. Chen, Y. Zhang, G. Xu, J. Yang and Y. Feng, *Particuology*, 2014, **15**, 27–33.

168 S. K. Meher and G. R. Rao, *J. Phys. Chem. C*, 2011, **115**, 25543–25556.

169 J. Wang, B. Niu, G. Du, R. Zeng, Z. Chen, Z. Guo and S. Dou, *Mater. Chem. Phys.*, 2011, **126**, 747–754.

170 C.-Y. Cao, W. Guo, Z.-M. Cui, W.-G. Song and W. Cai, *J. Mater. Chem.*, 2011, **21**, 3204–3209.

171 A. B. Corradi, F. Bondioli, B. Focher, A. M. Ferrari, C. Grippo, E. Mariani and C. Villa, *J. Am. Ceram. Soc.*, 2005, **88**, 2639–2641.

172 Y. Zhu, C. Cao, S. Tao, W. Chu, Z. Wu and Y. Li, *Sci. Rep.*, 2014, **4**, 5787.

173 J. Fang, M. Li, Q. Li, W. Zhang, Q. Shou, F. Liu, X. Zhang and J. Cheng, *Electrochim. Acta*, 2012, **85**, 248–255.

174 C.-C. Hu, C.-T. Hsu, K.-H. Chang and H.-Y. Hsu, *J. Power Sources*, 2013, **238**, 180–189.

175 J. Li, M. Wei, W. Chu and N. Wang, *Chem. Eng. J.*, 2017, **316**, 277–287.

176 Y. Tao, Z. Haiyan, L. Ruiyi, L. Zaijun, L. Junkang, W. Guangli and G. Zhiquo, *Electrochim. Acta*, 2013, **111**, 71–79.

177 J. Xu, Z. Ju, J. Cao, W. Wang, C. Wang and Z. Chen, *J. Alloys Compd.*, 2016, **689**, 489–499.

178 L. Xu, Y.-S. Ding, C.-H. Chen, L. Zhao, C. Rimkus, R. Joesten and S. L. Suib, *Chem. Mater.*, 2008, **20**, 308–316.

179 Y. Ren and L. Gao, *J. Am. Ceram. Soc.*, 2010, **93**, 3560–3564.

180 X. Liu, R. Ma, Y. Bando and T. Sasaki, *Angew. Chem.*, 2010, **122**, 8429–8432.

181 G. Chen, S. S. Liaw, B. Li, Y. Xu, M. Dunwell, S. Deng, H. Fan and H. Luo, *J. Power Sources*, 2014, **251**, 338–343.

182 M. Hussein, Z. Zainal and C. Y. Ming, *J. Mater. Sci. Lett.*, 2000, **19**, 879–883.

183 R. Kumar, W. C. Macedo, R. K. Singh, V. S. Tiwari, C. J. L. Constantino, A. Matsuda and S. A. Moshkalev, *ACS Appl. Nano Mater.*, 2019, **2**, 4626–4636.

184 R. Kumar, A. V. Alaferdov, R. K. Singh, A. K. Singh, J. Shah, R. K. Kotnala, K. Singh, Y. Suda and S. A. Moshkalev, *Composites, Part B*, 2019, **168**, 66–76.

185 N. H. Aminuddin Rosli, K. S. Lau, T. Winie, S. X. Chin and C. H. Chia, *Mater. Chem. Phys.*, 2021, **262**, 124274.

186 Domga, M. Karnan, F. Oladoyinbo, G. B. Noumi, J. B. Tchatchueng, M. J. Sieliechi, M. Sathish and D. K. Pattanayak, *Electrochim. Acta*, 2020, **341**, 135999.

187 A. A. B. Hamra, H. N. Lim, N. M. Huang, N. S. K. Gowthaman, H. Nakajima and M. M. Rahman, *J. Mol. Struct.*, 2020, **1220**, 128710.

188 S. Liu, S. Sarwar, H. Zhang, Q. Guo, J. Luo and X. Zhang, *Electrochim. Acta*, 2020, **364**, 137320.

189 L. Luo, Y. Zhou, W. Yan, X. Wu, S. Wang and W. Zhao, *Electrochim. Acta*, 2020, **360**, 137010.

190 C. Miao, X. Yin, G. Xia, K. Zhu, K. Ye, Q. Wang, J. Yan, D. Cao and G. Wang, *Appl. Surf. Sci.*, 2021, **543**, 148811.

191 P. Periasamy, T. Krishnakumar, V. P. Devarajan, M. Sandhiya, M. Sathish and M. Chavali, *Mater. Lett.*, 2020, **274**, 127998.

192 K.-d. Seong, X. Jin, D. Kim, J. M. Kim, D. Ko, Y. Cho, M. Hwang, J.-H. Kim and Y. Piao, *J. Electroanal. Chem.*, 2020, **874**, 114464.

193 Z. Tang, S. Tang, Q. Li, Z. Wei and T. Zhou, *J. Colloid Interface Sci.*, 2021, **582**, 312–321.

194 V. M. Vimuna, A. R. Athira, K. V. Dinesh Babu and T. S. Xavier, *Diamond Relat. Mater.*, 2020, **110**, 108129.

195 F. Zhao, D. Xie, W. Huang, X. Song, M. Aurang Zeb Gul Sial, H. Wu, F. Deng, Q. Zhang, J. Zou and X. Zeng, *J. Colloid Interface Sci.*, 2020, **580**, 160–170.

196 F. Zhao, D. Xie, X. Song, H. Wu, Q. Zhang, J. Zou and X. Zeng, *Appl. Surf. Sci.*, 2021, **539**, 148260.

197 Y. Kim, E.-s. Cho, S.-J. Park and S. Kim, *J. Ind. Eng. Chem.*, 2016, **33**, 108–114.

198 Y. Lin, D. W. Baggett, J.-W. Kim, E. J. Siochi and J. W. Connell, *ACS Appl. Mater. Interfaces*, 2011, **3**, 1652–1664.

199 A. Loupy, D. Monteux, A. Petit, J. M. Aizpurua, E. Domínguez and C. Palomo, *Tetrahedron Lett.*, 1996, **37**, 8177–8180.

200 T. J. Imholt, C. A. Dyke, B. Hasslacher, J. M. Perez, D. W. Price, J. A. Roberts, J. B. Scott, A. Wadhawan, Z. Ye and J. M. Tour, *Chem. Mater.*, 2003, **15**, 3969–3970.

201 S. C. Motshekga, S. K. Pillai, S. S. Ray, K. Jalama and R. W. M. Krause, *J. Nanomater.*, 2012, **2012**, 691503.

202 Z. Jian, P. Liu, F. Li, P. He, X. Guo, M. Chen and H. Zhou, *Angew. Chem., Int. Ed.*, 2014, **53**, 442–446.

203 J.-Y. Kim, K.-H. Kim, S.-H. Park and K.-B. Kim, *Electrochim. Acta*, 2010, **55**, 8056–8061.

204 Y. Guo, H. Wang, C. He, L. Qiu and X. Cao, *Langmuir*, 2009, **25**, 4678–4684.

205 D. Grekov, P. Pré and B. J. Alappat, *Renewable Sustainable Energy Rev.*, 2020, **124**, 109743.

206 L. L. Sikeyi, T. D. Ntuli, T. H. Mongwe, N. W. Maxakato, E. Carleschi, B. P. Doyle, N. J. Coville and M. S. Maubane-Nkadimeng, *Int. J. Hydrogen Energy*, 2021, **46**(18), 10862–10875.

207 H. Eskalen, S. Uruş, S. Cömertpay, A. H. Kurt and Ş. Özgan, *Ind. Crops Prod.*, 2020, **147**, 112209.

208 P. Kumar, G. Bhatt, R. Kaur, S. Dua and A. Kapoor, *Fullerenes, Nanotubes, Carbon Nanostruct.*, 2020, **28**, 724–731.

209 M. Pajewska-Szmyt, B. Buszewski and R. Gadzała-Kopciuch, *Mater. Chem. Phys.*, 2020, **242**, 122484.

210 X. Xia, C.-F. Cheng, Y. Zhu and B. D. Vogt, *Microporous Mesoporous Mater.*, 2021, **310**, 110639.

211 H. Qiu, X. Sun, S. An, D. Lan, J. Cui, Y. Zhang and W. He, *J. Colloid Interface Sci.*, 2020, **567**, 264–273.

212 M. Fu, Z. Zhu, W. Chen, H. Yu and Q. Liu, *J. Mater. Sci.*, 2020, **55**, 16385–16393.

213 V. Sannasi, K. U. Maheswari, C. Karthikeyan and S. Karuppuchamy, *Ionics*, 2020, **26**, 4067–4079.

214 A. Kumar, Y. Kuang, Z. Liang and X. Sun, *Mater. Today Nano*, 2020, 100076.

215 Y. Zhang, Q. Shao, C. Chen, H. Jiang, F. Su, Q. Hu and Z. Guo, *Powder Technol.*, 2020, **370**, 226–236.

216 M. Hashemzehi, V. Pirouzfar, H. Nayebzadeh and A. Alihosseini, *Adv. Powder Technol.*, 2020, **31**, 1470–1479.

217 I. M. Gonzaga, A. R. Dória, V. M. Vasconcelos, F. M. Souza, M. C. dos Santos, P. Hammer, M. A. Rodrigo, K. I. Eguiluz and G. R. Salazar-Banda, *J. Electroanal. Chem.*, 2020, **874**, 114460.

218 J. Cañón, M. Velasquez, R. Molina and S. Moreno, *Mol. Catal.*, 2020, **493**, 111080.

219 D. Y. Nadargi, M. S. Tamboli, S. S. Patil, R. B. Dateer, I. S. Mulla, H. Choi and S. S. Suryavanshi, *ACS Omega*, 2020, **5**, 8587–8595.

220 K. Kannan, D. Sivasubramanian, P. Seetharaman and S. Sivaperumal, *Optik*, 2020, **204**, 164221.

221 N. Thakur and K. Kumar, *J. Environ. Chem. Eng.*, 2020, **8**, 104011.

222 R. Kumar, S. M. Youssry, K. Z. Ya, W. K. Tan, G. Kawamura and A. Matsuda, *Diamond Relat. Mater.*, 2020, **101**, 107622.

223 A. J. Khan, M. S. Javed, M. Hanif, Y. Abbas, X. Liao, G. Ahmed, M. Saleem, S. Yun and Z. Liu, *Ceram. Int.*, 2020, **46**, 3124–3131.

224 K. Rao, K. Mahesh and S. Kumar, *Bull. Mater. Sci.*, 2005, **28**, 19–24.

225 S. Anandan and J. J. Wu, *Mater. Lett.*, 2009, **63**, 2387–2389.

226 C.-Y. Cao, Z.-M. Cui, C.-Q. Chen, W.-G. Song and W. Cai, *J. Phys. Chem. C*, 2010, **114**, 9865–9870.

227 L.-H. Ai and J. Jiang, *Powder Technol.*, 2009, **195**, 11–14.

228 H. Wang, J.-Z. Xu, J.-J. Zhu and H.-Y. Chen, *J. Cryst. Growth*, 2002, **244**, 88–94.

229 H. Katsuki and S. Komarneni, *J. Am. Ceram. Soc.*, 2001, **84**, 2313–2317.

230 V. Polshettiwar, B. Baruwati and R. S. Varma, *ACS Nano*, 2009, **3**, 728–736.

231 C. R. Patra and A. Gedanken, *New J. Chem.*, 2004, **28**, 1060–1065.

232 K. Wang, T. Huang, H. Liu, Y. Zhao, H. Liu and C. Sun, *Colloids Surf., A*, 2008, **325**, 21–25.

233 J.-J. Zhu, J.-M. Zhu, X.-H. Liao, J.-L. Fang, M.-G. Zhou and H.-Y. Chen, *Mater. Lett.*, 2002, **53**, 12–19.

234 X. Jia, W. He, X. Zhang, H. Zhao, Z. Li and Y. Feng, *Nanotechnology*, 2007, **18**, 075602.

235 A. Phuruangrat, D. J. Ham, S. J. Hong, S. Thongtem and J. S. Lee, *J. Mater. Chem.*, 2010, **20**, 1683–1690.

236 X. Hu, J. Gong, L. Zhang and J. C. Yu, *Adv. Mater.*, 2008, **20**, 4845–4850.

237 F. Bondioli, A. M. Ferrari, C. Leonelli, C. Siligardi and G. C. Pellacani, *J. Am. Ceram. Soc.*, 2001, **84**, 2728–2730.

238 H. Wu, M. Shao, J. Gu and X. Wei, *Mater. Lett.*, 2004, **58**, 2166–2169.

239 Y. Liu, Y. Hu, M. Zhou, H. Qian and X. Hu, *Appl. Catal., B*, 2012, **125**, 425–431.

240 N. P. Herring, S. H. Almahoudi, C. R. Olson and M. S. El-Shall, *J. Nanopart. Res.*, 2012, **14**, 1277.

241 Y. Tian, Y. Liu, W.-p. Wang, X. Zhang and W. Peng, *Electrochim. Acta*, 2015, **156**, 244–251.

242 S. Yan, H. Wang, P. Qu, Y. Zhang and Z. Xiao, *Synth. Met.*, 2009, **159**, 158–161.

243 J. Yan, Z. Fan, T. Wei, J. Cheng, B. Shao, K. Wang, L. Song and M. Zhang, *J. Power Sources*, 2009, **194**, 1202–1207.

244 M. Li, J. Cheng, J. Fang, Y. Yang, F. Liu and X. Zhang, *Electrochim. Acta*, 2014, **134**, 309–318.

245 C. R. Strauss and R. W. Trainor, *Aust. J. Chem.*, 1995, **48**, 1665–1692.

246 M. A. Surati, S. Jauhari and K. Desai, *Arch. Appl. Sci. Res.*, 2012, **4**, 645–661.

247 R. N. Gedye, F. E. Smith and K. C. Westaway, *Can. J. Chem.*, 1988, **66**, 17–26.

248 R. N. Gedye, W. Rank and K. C. Westaway, *Can. J. Chem.*, 1991, **69**, 706–711.

249 R. Gedye, F. Smith, K. Westaway, H. Ali and L. Baldisera, *Tetrahedron Lett.*, 1986, **27**, 279–282.

250 F. Shi, C. Li, M. Xia, K. Miao, Y. Zhao, S. Tu, W. Zheng, G. Zhang and N. Ma, *Bioorg. Med. Chem. Lett.*, 2009, **19**, 5565–5568.

251 T. H. Manjashetty, P. Yogeeswari and D. Sriram, *Bioorg. Med. Chem. Lett.*, 2011, **21**, 2125–2128.

252 J. Sedelmeier, S. V. Ley, H. Lange and I. R. Baxendale, *Eur. J. Org. Chem.*, 2009, **2009**, 4412–4420.

253 R. N. Baig and R. S. Varma, *Green Chem.*, 2013, **15**, 1839–1843.

254 H. Park, K. Y. Hwang, Y. H. Kim, K. H. Oh, J. Y. Lee and K. Kim, *Bioorg. Med. Chem. Lett.*, 2008, **18**, 3711–3715.

255 R. N. Baig and R. S. Varma, *Chem. Commun.*, 2012, **48**, 6220–6222.

256 B. R. Vaddula, R. S. Varma and J. Leazer, *Eur. J. Org. Chem.*, 2012, **2012**, 6852–6855.

257 X. Zhang, X. Sun, H. Zhang, D. Zhang and Y. Ma, *Electrochim. Acta*, 2013, **87**, 637–644.

258 S. Vijayakumar, A. K. Ponnalagi, S. Nagamuthu and G. Muralidharan, *Electrochim. Acta*, 2013, **106**, 500–505.

259 S. Wang and X. Wang, *Electrochim. Acta*, 2011, **56**, 3338–3344.

260 A. Devadas, S. Baranton, T. W. Napporn and C. Coutanceau, *J. Power Sources*, 2011, **196**, 4044–4053.

261 R. D. Kumar and S. Karuppuchamy, *Ceram. Int.*, 2014, **40**, 12397–12402.

262 X. She, X. Zhang, J. Liu, L. Li, X. Yu, Z. Huang and S. Shang, *Mater. Res. Bull.*, 2015, **70**, 945–950.

263 Y. Lei, J. Li, Y. Wang, L. Gu, Y. Chang, H. Yuan and D. Xiao, *ACS Appl. Mater. Interfaces*, 2014, **6**, 1773–1780.

264 N. I. Chandrasekaran and M. Manickam, *Int. J. Hydrogen Energy*, 2017, **42**, 26475–26487.

265 G. Xia and S. Wang, *Ceram. Int.*, 2019, **45**, 20810–20817.

266 J. J. William, I. M. Babu and G. Muralidharan, *Mater. Chem. Phys.*, 2019, **224**, 357–368.

267 M. Fu, Z. Zhu, Z. Zhang, Q. Zhuang, W. Chen and Q. Liu, *J. Alloys Compd.*, 2020, **846**, 156376.

268 M. Zhang, T. Ma, Y. Wang, D. Pan and J. Xie, *J. Mater. Sci.: Mater. Electron.*, 2018, **29**, 6991–7001.

269 J. Kim, Y. Jung and S. Kim, *Carbon Lett.*, 2019, **29**, 411–418.

270 Y. Zheng, Y. Tian, S. Liu, X. Tan, S. Wang, Q. Guo, J. Luo and Z. Li, *J. Alloys Compd.*, 2019, **806**, 170–179.

271 Y. Zheng, Y. Tian, H. Zhang, Q. Guo and J. Luo, *Inorg. Chem. Commun.*, 2019, **110**, 107596.

272 A. Y. Faid and H. Ismail, *Mater. Today Energy*, 2019, **13**, 285–292.

273 Y. Sun, X. Du, J. Zhang, N. Huang, L. Yang and X. Sun, *J. Power Sources*, 2020, **473**, 228609.

274 R. Kumar, R. K. Singh, A. R. Vaz, R. Savu and S. A. Moshkalev, *ACS Appl. Mater. Interfaces*, 2017, **9**, 8880–8890.

275 R. Kumar, R. K. Singh, P. K. Dubey, D. P. Singh and R. M. Yadav, *ACS Appl. Mater. Interfaces*, 2015, **7**, 15042–15051.

276 R. Kumar, R. K. Singh, R. Savu, P. K. Dubey, P. Kumar and S. A. Moshkalev, *RSC Adv.*, 2016, **6**, 26612–26620.

277 R. Kumar, R. K. Singh, A. V. Alaferdov and S. A. Moshkalev, *Electrochim. Acta*, 2018, **281**, 78–87.

278 R. Kumar, M. M. Abdel-Galeil, K. Z. Ya, K. Fujita, W. K. Tan and A. Matsuda, *Appl. Surf. Sci.*, 2019, **481**, 296–306.

279 M. Fu, Q. Zhuang, Z. Zhu, Z. Zhang, W. Chen, Q. Liu and H. Yu, *J. Alloys Compd.*, 2020, **862**, 158006.

280 R. Kumar, S. M. Youssry, M. M. Abdel-Galeil and A. Matsuda, *J. Mater. Sci.: Mater. Electron.*, 2020, **31**, 15456–15465.

281 J. Liu, X. Li, J. Yang, D. Geng, Y. Li, D. Wang, R. Li, X. Sun, M. Cai and M. W. Verbrugge, *Electrochim. Acta*, 2012, **63**, 100–104.

282 A. K. Rai, L. T. Anh, C.-J. Park and J. Kim, *Ceram. Int.*, 2013, **39**, 6611–6618.

283 S. Chen, Y. Zhao, B. Sun, Z. Ao, X. Xie, Y. Wei and G. Wang, *ACS Appl. Mater. Interfaces*, 2015, **7**, 3306–3313.

284 S. Baek, S.-H. Yu, S.-K. Park, A. Pucci, C. Marichy, D.-C. Lee, Y.-E. Sung, Y. Piao and N. Pinna, *RSC Adv.*, 2011, **1**, 1687–1690.

285 Y. Wang and J. Y. Lee, *J. Power Sources*, 2005, **144**, 220–225.

286 T. Muraliganth, A. V. Murugan and A. Manthiram, *Chem. Commun.*, 2009, 7360–7362.

287 W. Yang, L. Zhang, Y. Hu, Y. Zhong, H. B. Wu and X. W. Lou, *Angew. Chem.*, 2012, **124**, 11669–11672.

288 P. Kundu, C. Nethravathi, P. A. Deshpande, M. Rajamathi, G. Madras and N. Ravishankar, *Chem. Mater.*, 2011, **23**, 2772–2780.

289 K. M. Garadkar, L. A. Ghule, K. B. Sapnar and S. D. Dhole, *Mater. Res. Bull.*, 2013, **48**, 1105–1109.

290 A. Habibi, M. Jalaly, R. Rahmanifard and M. Ghorbanzadeh, *J. Alloys Compd.*, 2020, **834**, 155014.

291 M. Kheradmandfard, H. Minouei, N. Tsvetkov, A. K. Vayghan, S. F. Kashani-Bozorg, G. Kim, S. I. Hong and D.-E. Kim, *Mater. Chem. Phys.*, 2021, **262**, 124265.

292 Y. Liu, Y. Zhang, Y. Liu, J. Zhu, Z. Ge, Z. Li and Y. Chen, *Carbon*, 2021, **173**, 809–816.

293 S. Pindar and N. Dhawan, *Sustainable Mater. Technol.*, 2020, **25**, e00157.

294 S. Pindar and N. Dhawan, *Process Saf. Environ. Prot.*, 2021, **147**, 226–233.

295 P. H. Salame and M. Devakar, *Ceram. Int.*, 2020, **46**, 28844–28850.

296 A. Uctepe, E. Demir, B. Tekin, B. Dursun, O. Ozturk, O. Sel and R. Demir-Cakan, *Solid State Ionics*, 2020, **354**, 115409.

297 S. Wang, Y. Zhu, X. Sun, S. An, J. Cui, Y. Zhang and W. He, *Colloids Surf., A*, 2021, **615**, 126276.

298 X. Wang, Z. Liu, Y. Tang, J. Chen, D. Wang and Z. Mao, *J. Power Sources*, 2021, **481**, 228924.

299 E. Zhang, B. Wang, J. Wang, H. Ding, S. Zhang, H. Duan, X. Yu and B. Lu, *Chem. Eng. J.*, 2020, **389**, 124407.

300 J. Zhang, A. Tahmasebi, J. E. Omoriyekomwan and J. Yu, *Fuel Process. Technol.*, 2021, **213**, 106714.

301 Y. Zhao, B. Liu, L. Zhang and S. Guo, *J. Hazard. Mater.*, 2020, **384**, 121487.

302 Y. Zhao, B. Liu, L. Zhang and S. Guo, *J. Hazard. Mater.*, 2020, **396**, 122740.

303 N. Zhou, W. Qin, C. Wu and C. Jia, *J. Alloys Compd.*, 2020, **834**, 155073.

304 Y. Fu, Y. He, Y. Yang, L. Qu, J. Li and R. Zhou, *J. Alloys Compd.*, 2020, **832**, 154920.

305 M. Liu, Q. Zhao, H. Liu, J. Yang, X. Chen, L. Yang, Y. Cui, W. Huang, W. Zhao, A. Song, Y. Wang, S. Ding, Y. Song, G. Qian, H. Chen and F. Pan, *Nano Energy*, 2019, **64**, 103942.

306 C.-H. Lu, N. Naresh, P. S. Kumar and S. Som, *Ceram. Int.*, 2019, **45**, 19517–19521.

307 Z. W. Lu, Y. H. Wang, Z. Dai, X. P. Li, C. Y. Zhang, G. Z. Sun, C. S. Gong, X. J. Pan, W. Lan, J. Y. Zhou and E. Q. Xie, *Electrochim. Acta*, 2019, **325**, 134920.

308 S. Wang, Y. Zhu, X. Sun, H. Liu, J. Cui, Y. Zhang and W. He, *Inorg. Chem. Commun.*, 2020, **121**, 108188.

309 J. Wu, J. Zhao, B. Vaidhyanathan, H. Zhang, A. Anshuman, A. Nare and S. Saremi-Yarahmadi, *Materialia*, 2020, **13**, 100833.

310 S. Yang, F. Ji, Z. Wang, Y. Zhu, K. Hu, Y. Ouyang, R. Wang, X. Ma and C. Cao, *Electrochim. Acta*, 2019, **324**, 134864.

311 X. Yang, Y. Tian, S. Sarwar, M. Zhang, H. Zhang, J. Luo and X. Zhang, *Electrochim. Acta*, 2019, **311**, 230–243.

312 C. Zhang, B. Zheng, Z. Song, S. Shi and H. Mao, *Ceram. Int.*, 2020, **46**, 1018–1025.

313 J. C.-Y. Jung, P.-C. Sui and J. Zhang, *J. Energy Storage*, 2021, **35**, 102217.

314 P. Lyu, X. Liu, J. Qu, J. Zhao, Y. Huo, Z. Qu and Z. Rao, *Energy Storage Mater.*, 2020, **31**, 195–220.

315 X. Wang, X. Wei, J. Zhu, H. Dai, Y. Zheng, X. Xu and Q. Chen, *eTransportation*, 2021, **7**, 100093.

316 X. Zhang, X. Sun, X. Li, X. Hu, S. Cai and C. Zheng, *J. Energy Chem.*, 2021, **59**, 343–363.

317 S. Zhao, Z. Guo, K. Yan, S. Wan, F. He, B. Sun and G. Wang, *Energy Storage Mater.*, 2021, **34**, 716–734.

318 P. Zhu, D. Gastol, J. Marshall, R. Sommerville, V. Goodship and E. Kendrick, *J. Power Sources*, 2021, **485**, 229321.

319 Y. Kang, Y.-H. Zhang, Q. Shi, H. Shi, D. Xue and F.-N. Shi, *J. Colloid Interface Sci.*, 2021, **585**, 705–715.

320 S. Liu, P. Yan, H. Li, X. Zhang and W. Sun, *Front. Chem.*, 2020, **8**, 104.

321 J.-H. Koo and S.-M. Paek, *Nanomaterials*, 2021, **11**, 319.

322 H. A. Tariq, J. J. Abraham, R. A. Shakoor, S. Al-Qaradawi, M. R. Abdul Karim and U. Chaudhry, *Energy Storage*, 2020, **2**, e202.

323 B. Dursun, E. Topac, R. Alibeyli, A. Ata, O. Ozturk and R. Demir-Cakan, *J. Alloys Compd.*, 2017, **728**, 1305–1314.

324 D. Li, D. Yan, J. Ma, W. Qin, X. Zhang, T. Lu and L. Pan, *Ceram. Int.*, 2016, **42**, 15634–15642.

325 X. Liu, T. Chen, H. Chu, L. Niu, Z. Sun, L. Pan and C. Q. Sun, *Electrochim. Acta*, 2015, **166**, 12–16.

326 Y. Mao, X. Zhang, Y. Zhou and W. Chu, *Scr. Mater.*, 2020, **181**, 92–96.

327 W. Qin, T. Chen, T. Lu, D. H. C. Chua and L. Pan, *J. Power Sources*, 2016, **302**, 202–209.

328 Z.-J. Zhang, Y.-X. Wang, S.-L. Chou, H.-J. Li, H.-K. Liu and J.-Z. Wang, *J. Power Sources*, 2015, **280**, 107–113.